# Global control of merging by the interplanetary magnetic field: Cluster observations of dawnside flank magnetopause reconnection

S. Eriksson,[1] S. R. Elkington,[1] T. D. Phan,[2] S. M. Petrinec,[3] H. Rème,[4] M. W. Dunlop,[5] M. Wiltberger,[6] A. Balogh,[7] R. E. Ergun,[1] and M. André[8]

Received 4 December 2003; revised 30 August 2004; accepted 22 September 2004; published 4 December 2004.

[1] Detailed Cluster observations of flank magnetopause reconnection are presented for two events on the Northern and the Southern Hemispheric dawnside flanks when the interplanetary magnetic field (IMF) clock angle $\theta = \arctan(B_y/B_z)$ is within $\sim 45°$ of the equatorial plane. The event selection is based on the relative proximity between the Cluster spacecraft 1 position and the predicted magnetospheric sash where antiparallel merging is expected to develop. MHD simulations performed for the two events indicate that the Cluster spacecraft were passing through the MHD sash region in the Northern Hemisphere on 30 June 2001, while crossing the magnetopause equatorward of the Southern Hemispheric sash on 29 May 2001. Accelerated and decelerated plasma flows relative to the magnetosheath velocity were detected by Cluster on both occasions. The Walén test confirms that the observed $\Delta\mathbf{V}$ is directly correlated with the predicted magnetic field rotation $\Delta\mathbf{B}/\sqrt{\rho\mu_0}$ with the expected direction of the normal magnetic field and so we interpret them as speed changes due to magnetic reconnection. The observed directions of $\Delta\mathbf{V}$ compare very well with the location of the simulated MHD sash relative to Cluster. The magnetic field shear in the locally tangential plane of the magnetopause ranges between 171° and 177° for the 30 June event in good agreement with antiparallel merging at the MHD sash. The corresponding local field shear for the 29 May event is only 144°, either suggesting a component merging site in the direction of the sash or indicating that Cluster is farther away from the location where the neutral line was initially formed as compared with the 30 June event. A comparison between the projected regions of antiparallel and component merging onto the magnetopause and the quasi-steady direction of plasma acceleration detected by Cluster on 29 May and 30 June support the view that the IMF controls the expected global location of magnetic reconnection at limited regions of the magnetopause. This is in contrast to randomly distributed merging sites over the dayside magnetopause that in principle could generate accelerated flows away from the observed directions of $\Delta\mathbf{V}$. *INDEX TERMS:* 2724 Magnetospheric Physics: Magnetopause, cusp, and boundary layers; 2740 Magnetospheric Physics: Magnetospheric configuration and dynamics; 2784 Magnetospheric Physics: Solar wind/magnetosphere interactions; 7835 Space Plasma Physics: Magnetic reconnection; *KEYWORDS:* flank magnetic reconnection, MHD sash

**Citation:** Eriksson, S., S. R. Elkington, T. D. Phan, S. M. Petrinec, H. Rème, M. W. Dunlop, M. Wiltberger, A. Balogh, R. E. Ergun, and M. André (2004), Global control of merging by the interplanetary magnetic field: Cluster observations of dawnside flank magnetopause reconnection, *J. Geophys. Res.*, *109*, A12203, doi:10.1029/2003JA010346.

[1]Laboratory for Atmospheric and Space Physics, University of Colorado, Boulder, Colorado, USA.
[2]Space Sciences Laboratory, University of California, Berkeley, California, USA.
[3]Lockheed Martin Advanced Technology Center, Palo Alto, California, USA.
[4]Centre d'Etude Spatiale des Rayonnements, Toulouse, France.
[5]Rutherford Appleton Laboratory, Chilton, UK.
[6]High Altitude Observatory, National Center for Atmospheric Research, Boulder, Colorado, USA.
[7]Imperial College, London, UK.
[8]Swedish Institute of Space Physics, Uppsala, Sweden.


0148-0227/04/2003JA010346$09.00

## 1. Introduction

[2] Reconnection between the magnetic fields of the magnetosheath and the geomagnetic field is an important process for the transfer of mass, energy, and momentum across the magnetopause [*Dungey*, 1961]. Evidence of reconnection in terms of accelerated plasma jets has since been observed in situ by several spacecraft and at various locations on the magnetopause [e.g., *Paschmann et al.*, 1979; *Sonnerup et al.*, 1981; *Gosling et al.*, 1991; *Kessel et al.*, 1996; *Avanov et al.*, 2001; *Phan et al.*, 2001].

[3] Several competing models exist, however, concerning the location of reconnection at the magnetopause. These

may be separated into two classes according to whether the primary criterion of the distribution of the merging sites is determined by the direction of the IMF or by locally satisfied criteria. The former class generally predicts limited regions over the magnetopause where reconnection may occur if the conditions are also locally satisfied, whereas the latter class suggests a more random distribution of merging sites [e.g., *Nishida*, 1989].

[4] There are two major categories of the IMF-dependent class of models. Either the merging site is given by the locus of approximate antiparallel alignment between the direction of the magnetic fields external and internal to the magnetosphere or it is found along a tilted line that passes through the subsolar region (the tilt depending on the IMF clock angle) where the merging fields form an angle $\theta \neq 180°$. These two hypotheses are referred to as the antiparallel model [*Crooker*, 1979; *Luhmann et al.*, 1984] and the component merging model [*Sonnerup*, 1974; *Gonzalez and Mozer*, 1974]. The reconnection sites are the same for both models when the IMF is either purely southward or northward but differ for intermediate clock angles [e.g., *Lockwood et al.*, 2003; *Petrinec and Fuselier*, 2003]. Although the exact location of the merging site differs between these two models, it should be noted that they are indeed limited in their extension over the magnetopause and controlled primarily by the IMF.

[5] The "magnetospheric sash" is predicted from magnetohydrodynamic (MHD) simulations [e.g., *White et al.*, 1998; *Maynard et al.*, 2001] and three-dimensional (3-D) electromagnetic kinetic codes [*Nishikawa*, 1998, and references therein] as a region of localized minima in the magnetic field magnitude that extends along the magnetopause. In general, it stretches downtail along the Northern Hemisphere dawnside (duskside) and the Southern Hemisphere duskside (dawnside) magnetopause when the IMF $B_y$ component is negative (positive) and eventually merges with the neutral sheet at some further distance downtail. *Siscoe et al.* [2001] compared the IMF dependence of the MHD sash clock angle in the $x_{GSM} = 0$ plane with the clock angle of the antiparallel merging site from the results of a vacuum superposition of a uniform IMF onto the geomagnetic field [e.g., *Yeh*, 1976; *Luhmann et al.*, 1984] and showed that they correspond to a "remarkable degree" considering that the superposition of the magnetic fields alone excludes the presence of plasma. To a first approximation, the location of the sash thus corresponds to the region of predicted antiparallel merging.

[6] The present event study examines Cluster observations [e.g., *Escoubet et al.*, 2001] from spacecraft 1 (C1) during two separate dawnside flank magnetopause crossings, when both accelerated and decelerated plasma flow velocities were detected in a locally depleted boundary layer [*Sonnerup et al.*, 1981] with a lower density than in the magnetosheath proper. These occurred in the Northern Hemisphere (NH) on 30 June 2001 and in the Southern Hemisphere (SH) on 29 May 2001. The events were selected by using an equation for the dayside antiparallel separator line [e.g., *Yeh*, 1976; *Crooker et al.*, 1990] suggesting that Cluster passed near the sash (section 2). However, since the applied expression is only valid in the $x_{GSM} = 0$ plane, we perform an MHD simulation for each of these dates using the Lyon-Fedder-Mobarry (LFM) code to correctly determine the relative direction between the sash and the location of C1. An overview of the LFM MHD code is given in Appendix A [see also *Wiltberger et al.*, 2000]. Assuming that the velocity changes $\Delta\mathbf{V}$ relative to the magnetosheath are due primarily to the $\mathbf{j} \times \mathbf{B}$ force generated by reconnection, we then compare the $\Delta\mathbf{V}$ directions measured at C1 with the predicted location of the MHD sash region where antiparallel merging is expected to develop (sections 3–5).

## 2. Event Selection Procedure

[7] The vacuum superposition model of a uniform external field with the internal dipole field results in a dayside antiparallel separator line, whose clock angle dependence on the IMF direction in the $x_{GSM} = 0$ plane was given explicitly by *Yeh* [1976] and later restated by *Crooker et al.* [1990] as

$$\tan(\theta_s) = -\left(3 \pm \sqrt{9 + 8\tan^2\left(\theta_{imf}\right)}\right)/2\tan\left(\theta_{imf}\right). \quad (1)$$

The minus (plus) sign applies for northward (southward) IMF $B_z$ conditions and the IMF clock angle is defined as $\theta_{imf} = \arctan(B_y/B_z)$ so that $\theta_{imf} = 0°$ and $\theta_{imf} = 90°$ correspond to the positive $z_{GSM}$ and $y_{GSM}$ directions, respectively. On the basis of the results of *Siscoe et al.* [2001] we assume that the clock angle of the sash corresponds to the clock angle of the separator line $\theta_s$ at $x_{GSM} = 0$. MHD simulations predict the presence of two sash regions on the magnetopause, one for each hemisphere. Since the given expression only provides the clock angle of the sash in the NH, we assume that the SH clock angle is given by $\theta_{south} = \theta_{north} + 180°$.

[8] The search for Cluster events that may coincide with the sash is performed as follows. It is first assumed that C1 will cross the magnetopause near the sash within a GSM region bounded by $-10\ R_E < x < 3\ R_E$ and $10\ R_E < R_{yz} < 20\ R_E$, where $R_{yz}^2 = y^2 + z^2$ is the radial distance in the $yz_{GSM}$ plane [e.g., *Shue et al.*, 1998]. The relative location of the predicted sash to Cluster within this critical volume of space is estimated by using the propagated IMF clock angle data from ACE as input to equation (1).

[9] The propagation time from ACE is calculated by assuming an average magnetopause location at $x = 10\ R_E$ and using the $x$ components of solar wind velocity and upstream spacecraft position. This first-order estimate excludes the additional time delays introduced by the subsonic velocity regime in the magnetosheath and by the finite time lag from the subsolar point at $x = 10\ R_E$ to the actual downwind Cluster transition region across the magnetopause. These delays are expected to be on the order of 5 to 10 min. It is moreover observed that the clock angle of the sash increases downtail from the $x = 0$ plane, where equation (1) is valid [*Siscoe et al.*, 2001]. The search is therefore limited to those instances when the clock angle of the C1 $yz_{GSM}$ position is within 10° of the predicted sash in either hemisphere.

[10] The Cluster spacecraft cross the $R_{yz} = 10\ R_E$ boundary on the dawnside flank in either hemisphere each May and June, while crossing the duskside flanks each November and December. The black section in Figure 1a

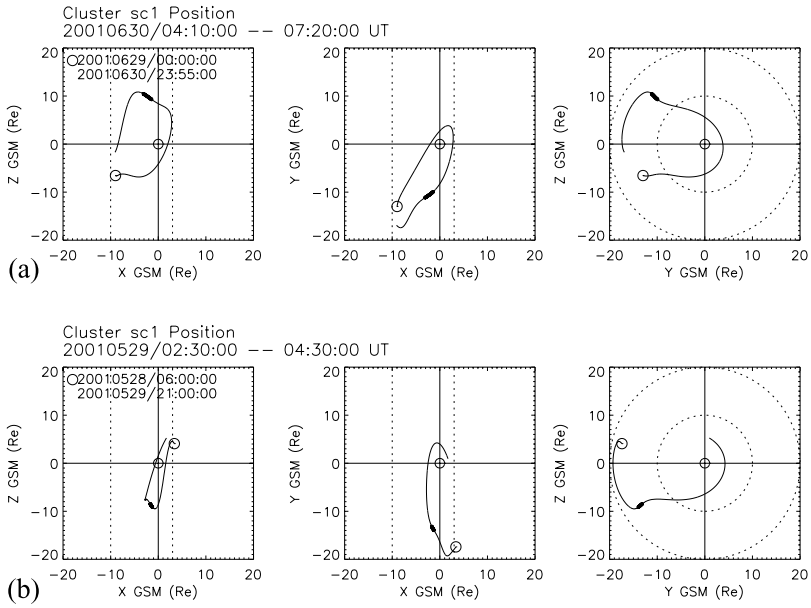


**Figure 1.** The C1 orbits are illustrated for two events in GSM coordinates that demonstrate the critical volume of space (dashed lines and circles) where Cluster is predicted to cross the magnetopause near the MHD sash. (a) From 0410 UT to 0720 UT on 30 June 2001 as indicated by the solid black section along the orbit. (b) From 0230 UT to 0430 UT on 29 May 2001 (black section). Thin solid lines indicate the orbit for the broader time interval which is shown explicitly in each *xz* plane projection. Large circles mark the start point of each time interval and indicate the direction of motion.

displays the period of one such dawnside event near the predicted sash in the NH between 0410 UT and 0720 UT on 30 June 2001. Another dawnside event is selected for analyses in the SH between 0230 UT and 0430 UT on 29 May 2001 (black section in Figure 1b). The following sections present detailed observations using C1 data in the context of antiparallel merging which is predicted to occur in the low-magnetic field regions of the simulated MHD sash. The geocentric solar magnetospheric (GSM) coordinate system is used throughout this study or otherwise stated explicitly.

## 3. Northern Hemisphere 30 June Event

[11] Figure 2a shows the C1 position in clock angle and radius in the *yz* plane versus its *x* position between 0300 UT and 0900 UT on 30 June 2001. The solid black dots represent the first time of entry in this interval. It is observed that the Cluster spacecraft move radially outward at a clock angle of $\theta \sim -46°$ while moving downtail from $x = -0.7\ R_E$ to $x = -4.0\ R_E$. Figure 2b displays the IMF components and the IMF clock angle recorded by the ACE spacecraft during the approximate time interval that corresponds to this segment of the Cluster orbit. The estimated propagation time is ~69 min from the ACE position at (247.5, 21.1, 14.4) $R_E$ (GSE coordinates) to the approximate subsolar magnetopause region and the time is in minutes relative to the ACE observations. Note that the IMF is dominated by a negative $B_y$ component during most of this period.

[12] The observed IMF clock angle data are then used to estimate the corresponding clock angle of the northern sash for this event as predicted by equation (1). Figure 2c displays the resulting clock angles of the IMF (solid dot), the northern sash (diamond), the southern sash (triangle), and the Cluster position (square). It is seen that C1 occasionally passes within 10° of the predicted sash in the NH as indicated by the small vertical bars along the time axis. We will later examine the actual proximity of C1 to the MHD sash in a simulation based on the LFM code.

### 3.1. Cluster Observations

[13] The C1 spin resolution (4 s) plasma data from the Hot Ion Analyzer (HIA) of the CIS instrument [*Rème et al.*, 2001] and the magnetic field data from the FGM instrument [*Balogh et al.*, 2001] are shown in a 6-hour long interval from 0400 UT in Figure 3. The successive panels from the top display the ion energy-time spectrogram (all pitch angles), the plasma density (assuming 100% $H^+$), the magnitude and individual GSM components of the ion velocity, the GSM components and magnitude of the magnetic field, and the Alfvén Mach number derived from the measured Alfvén velocity,

$$M_A = V/V_A = V\sqrt{Nm_p\mu_0}/B, \tag{2}$$

where $V$ and $B$ are the total velocity and magnetic field, respectively, $N$ is the $H^+$ density, and $m_p$ is the proton rest mass.

[14] There are several magnetopause crossings during the 6-hour time period in Figure 3. A clear outbound traversal into the magnetosheath occurs at ~0420 UT as suggested by the increase in plasma density and flow velocity. An increase of magnetosheath ion energy fluxes is also seen between 50 eV and ~900 eV in the energy-time spectrogram. Cluster then stays in the magnetosheath until ~0915 UT, except for a limited number of magnetopause traversals such as the

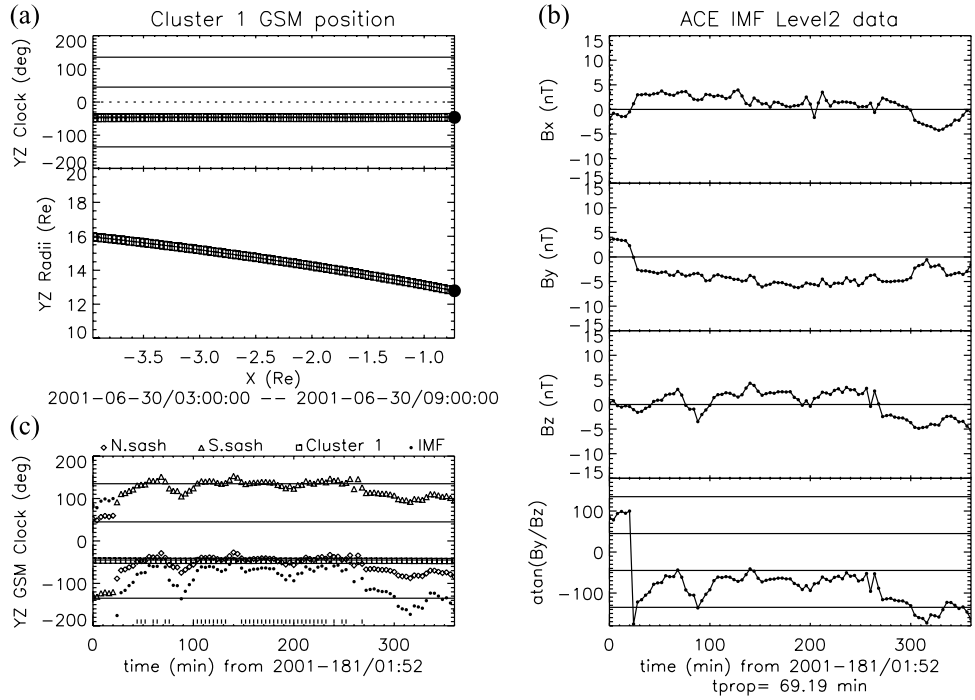


**Figure 2.** (a) C1 clock angle in the *yz* plane (top) and the *yz* radial position (bottom) versus *x* position from 0300 UT (solid dot) to 0900 UT on 30 June 2001. (b) The ACE IMF data versus time at ACE corresponding to the C1 interval. The propagation time is ∼69 min. (c) The clock angles of the IMF (solid dot), the northern sash using equation (1) (diamond), the southern sash (triangle), and the C1 position (square) indicating when C1 is within 10° of the predicted sash (vertical marks along time axis).

ones at ∼0623 UT and ∼0711 UT. The magnetosheath between 0440 UT and 0740 UT is also characterized by an average Alfvén Mach number of $M_A = 2.0$.

[15] The ion velocity data indicate the presence of several plasma flow enhancements and periods of decelerated flows relative to a more gradually varying magnetosheath velocity. These occur intermittently between 0440 UT and ∼0750 UT. Prior to performing any detailed analysis of these flow events, however, we employ the minimum variance analysis (MVA) technique on the magnetic field between 0547:10 UT and 0553:10 UT (blue vertical lines in Figure 3). The magnetic field during this interval rotates from an approximate geomagnetic field-like direction toward its magnetosheath direction, suggesting a transition of the magnetopause.

[16] The MVA technique [*Sonnerup and Scheible*, 1998] applied to magnetic field data from a single spacecraft can provide an estimate for the direction normal to a one-dimensional current layer, wave front, or transition layer in the plasma such as a magnetopause crossing. The resulting eigenvalues from the MVA analysis are $\lambda_1 = 164.00$, $\lambda_2 = 42.65$, and $\lambda_3 = 3.43$, respectively. The ratio of intermediate to minimum eigenvalues equals 12.45, which indicates a good determination of the minimum variance direction and hence a good estimate for the boundary normal determination [e.g., *Sonnerup*, 1971; *Sonnerup et al.*, 1987; *Phan et al.*, 2001]. The resulting magnetopause normal in GSM is then given by the eigenvector $\hat{\mathbf{n}}$ = (0.41, −0.60, 0.68) corresponding to $\lambda_3$. The two remaining eigenvectors span the locally tangential plane of the magnetopause. We rotate these unit vectors in this plane so that one vector is aligned in the westward direction of the $xy_{GSM}$ plane and the other in the approximate direction of the positive $z_{GSM}$ axis [e.g., *Russell and Elphic*, 1979]. The latter is defined as the $\hat{\mathbf{l}}$ direction, while $\hat{\mathbf{m}} = \hat{\mathbf{n}} \times \hat{\mathbf{l}}$ points westward. Here, $\hat{\mathbf{l}}$ = (−0.38, 0.57, 0.73), while $\hat{\mathbf{m}}$ is given as $\hat{\mathbf{m}}$ = (−0.83, −0.56, 0.00).

[17] Figure 4 shows the C1 data between 0410 UT and 0720 UT where the ion velocity and the magnetic field (see Figure 3) have been transformed into the LMN boundary normal frame of reference by using the obtained unit vectors $\hat{\mathbf{n}}$, $\hat{\mathbf{l}}$, and $\hat{\mathbf{m}}$. A number of enhanced and reduced speed intervals are clearly observed in the velocity magnitude measurements (second panel from the top) during this event, some of which are indicated between pairs of dashed vertical lines. These plasma jets generally experience speed changes primarily along the east-west $\hat{\mathbf{m}}$ direction and occur as the magnetic field rotates between a westward magnetosheath direction ($B_m > 0$) and the eastward direction ($B_m < 0$) expected on the earthward side of the NH dawn-side flank magnetopause. We also find that the jets most often display $\Delta\mathbf{V}$ changes in the negative $\hat{\mathbf{l}}$ direction as compared with the generally poleward directed magnetosheath velocity at $V_l \sim 80$ km/s.

[18] The solid vertical lines in Figure 4 mark the onset of several plasma density depletion intervals where the magnetosheath density is reduced from ∼20 cm$^{-3}$ to ∼10 cm$^{-3}$. It seems that most plasma jets are observed within such depleted regions or near the boundary with the higher-density magnetosheath proper. The depleted regions are likely the signature of the proposed plasma boundary layer [see *Sonnerup et al.*, 1981, Figure 1a] on the earthward

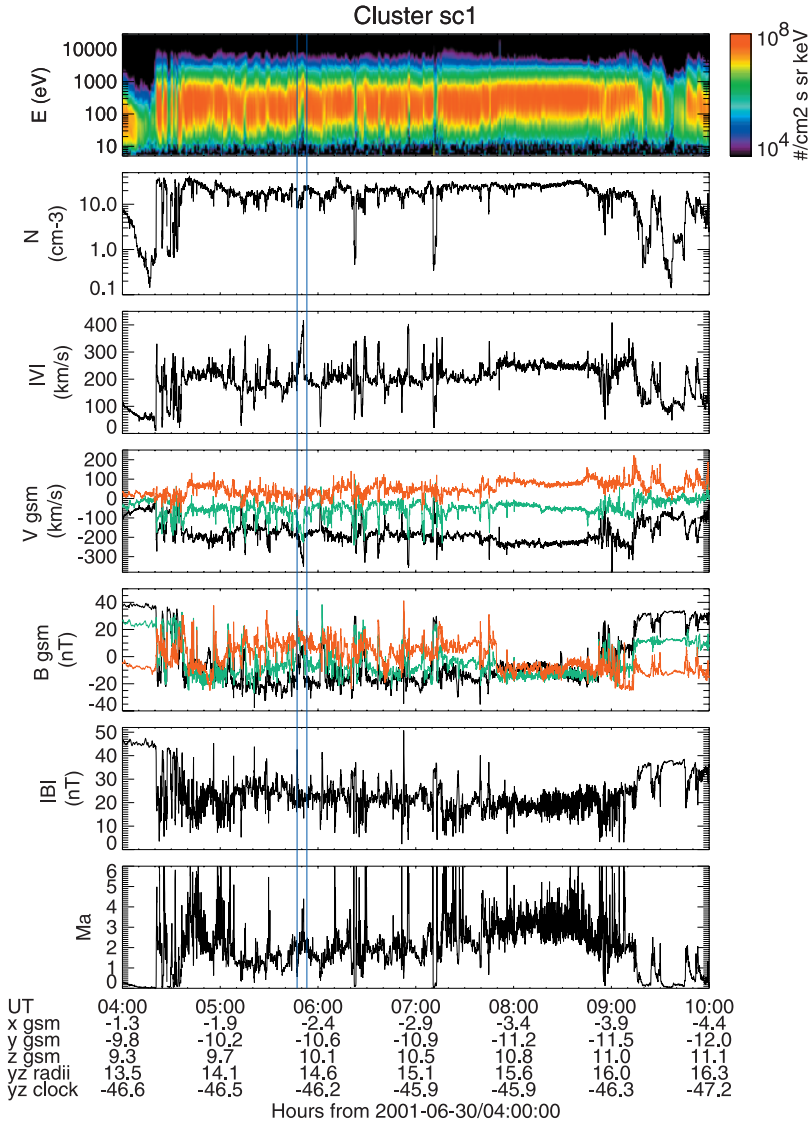


**Figure 3.** C1 spin resolution CIS data from the HIA instrument and magnetic field data from the FGM instrument are shown between 0400 UT and 1000 UT on 30 June 2001. Panels from the top display the ion energy-time spectrogram, the ion density in $cm^{-3}$, the magnitude and GSM components of the ion velocity, the GSM components and magnitude of the magnetic field, and the Alfvén Mach number. The $x_{GSM}$, $y_{GSM}$, and $z_{GSM}$ components in velocity and magnetic field are shown in black, green, and red, respectively. The time and position of these Cluster observations from the NH dawnside flank magnetosphere are shown below the panels, including the Cluster radial and clock angle position. Blue vertical lines mark the time period of the minimum variance analysis (see text for details). The magnetosheath is characterized by a plasma density of $\sim$20 $cm^{-3}$ and an ion speed of $\geq$200 km/s.

side of the magnetopause in the vicinity of magnetic reconnection sites.

[19] Magnetic reconnection at the magnetopause generates a rotational discontinuity in the magnetic field with a nonzero normal component present across the magnetopause. The discontinuity, which may also be described as an intermediate shock, is predicted to propagate away from the diffusion region at the magnetic field-aligned Alfvén velocity in the deHoffmann-Teller (HT) shock frame of reference [*deHoffmann and Teller*, 1950; *Khrabrov and Sonnerup*, 1998]. Whether the plasma is accelerated to the Alfvén velocity by the intermediate shock or not may be tested in a component-by-component scatterplot of the observed $\mathbf{V} - \mathbf{V}_{HT}$ against the locally measured $\mathbf{V}_A$ which is also referred to as the Walén test [e.g., *Sonnerup et al.*, 1990]. This test should be performed so that the chosen interval includes a set of measurements on either side of the magnetopause boundary [*Khrabrov and Sonnerup*, 1998] as identified by the different directions of the magnetic fields. The downstream side is characterized by higher (or lower) velocities than observed in the incident upstream magnetosheath flow.

[20] The time intervals between the dashed lines in Figure 4 were selected in this way and include observations on either side of the magnetopause. Figure 5 illustrates the Walén tests in the HT frame for these time periods.

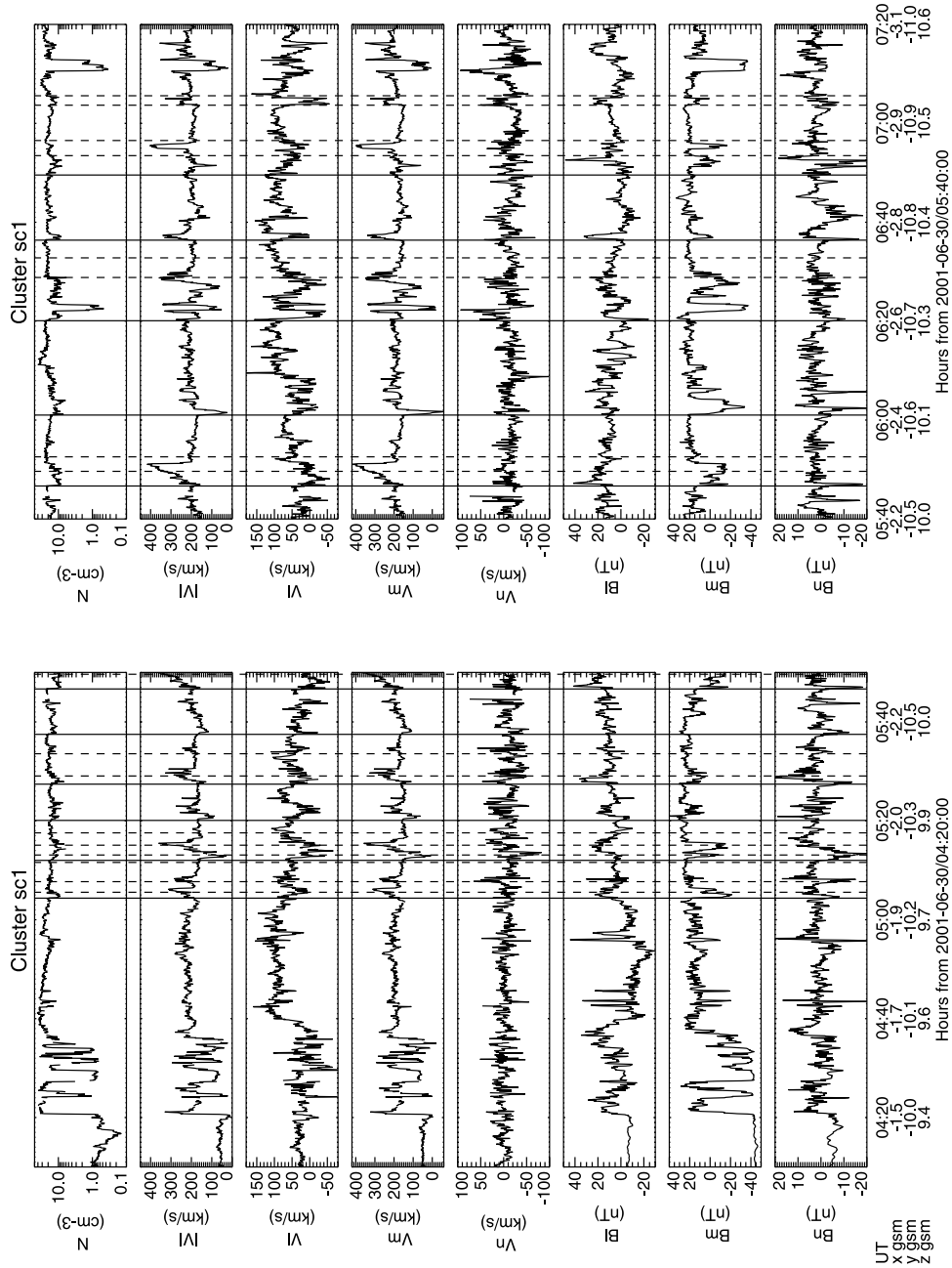


**Figure 4.** C1 data on 30 June 2001 from 0410 UT to 0720 UT. Ion velocity and magnetic field vectors have been transformed into the estimated LMN boundary normal system using the minimum variance analysis on the magnetic field data (see text for details). Dashed vertical lines indicate a total of eight plasma jet intervals where the Walén relation [e.g., *Khrabrov and Sonnerup*, 1998] is tested. The solid vertical lines mark the onset of a selected number of plasma depletion intervals.

The HT velocity in each of these intervals is derived using the method developed by *Sonnerup et al.* [1987]. They also provided a quantitative measure of fit for the HT velocity given by the $D/D_0$ ratio, where the following expression,

$$D = \frac{1}{N}\sum_{j=1}^{N} \left|\left(\mathbf{V}^j - \mathbf{V}_{HT}\right) \times \mathbf{B}^j\right|^2, \tag{3}$$

is to be minimized and $D_0$ is evaluated by setting $\mathbf{V}_{HT} = 0$. The superscript $j$ is used to denote the $N$ individual data points in the chosen time series interval. The smaller $D/D_0$ is, the better the expected quality of the HT frame.

[21] The HT velocity $\mathbf{V}_{HT}$ in GSM coordinates and the $D/D_0$ ratio together with the best fit slope and the correlation coefficient are given explicitly for all the eight time periods displayed in Figure 5. Six of the selected plasma jet intervals display negative Walén slopes between 90% and 100% of the local Alfvén speed $V_A$ with correlation coefficients ranging from cc = −0.93 to cc = −0.97. This is in good agreement with theoretical predictions of reconnection.

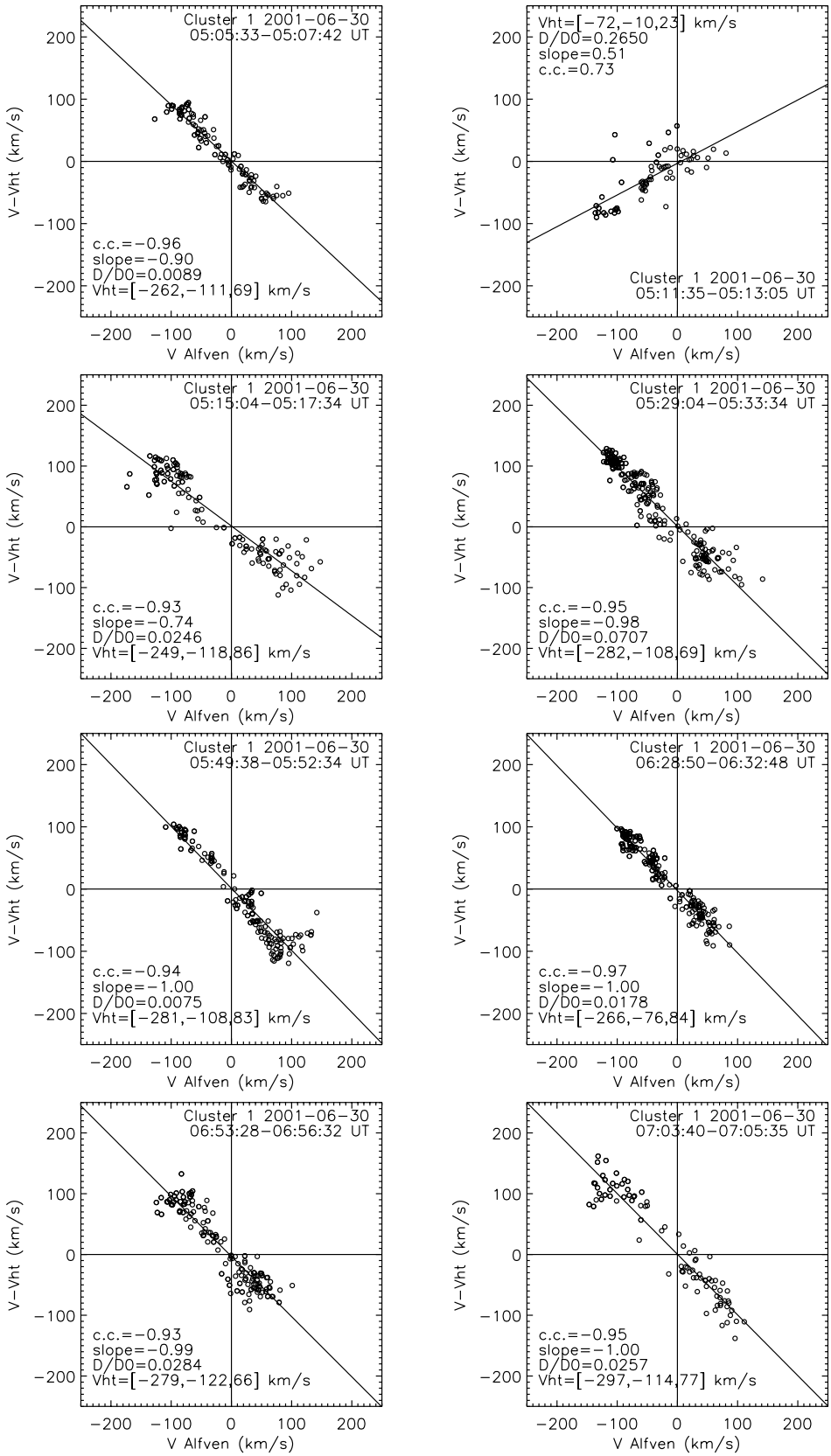


**Figure 5.** Walén analyses for eight time periods on 30 June 2001 as displayed in Figure 4. The flow velocity vector in the HT frame is shown versus the Alfvén velocity vector. The correlation coefficient, the best fit slope, the quality ratio of the HT frame $D/D_0$, and the HT velocity are all shown explicitly for each time period. The negative (positive) slopes indicate that these observations were detected tailward (sunward) of a reconnection X-line.

[22] There are two jet intervals, however, separated by about 2 min that seemingly fail the Walén test in the HT frame. The first interval centered near 0512 UT indicates that this decelerated flow event has a positive regression slope in the HT frame at just 51% of $V_A$ and a lower correlation coefficient of about cc = 0.73. The subsequent accelerated flow event around 0516 UT display a higher correlation (cc = −0.93) negative slope at 74% of $V_A$. An examination of $\mathbf{V} \times \mathbf{B}$ and $\mathbf{V}_{HT} \times \mathbf{B}$ for the 0512 UT event (not shown) show that the quality of the HT frame is comparable with those during the tailward accelerated flow events in Figure 5. A major difference, however, is the peak amplitude of the estimated convective electric fields. These are on the order of ±1.5 mV/m for the 0512 event but peak near ±5.0 mV/m for the negative slope event around 0550 UT in Figure 5. This difference is likely due to the different magnitudes of the plasma velocity during these time intervals.

[23] Analyses of another four decelerated flow events near 0521 UT, 0538 UT, 0601 UT, and 0651 UT (see Figure 4) result in positive slopes with correlation coefficients and slope magnitudes comparable to the 0512 UT event. The deviation from fully Alfvénic field-aligned flows in the HT frame of reference during these time intervals may suggest the presence of more complex two-dimensional or three-dimensional magnetic field structures than that assumed in the HT frame analysis [*Sonnerup et al.*, 1990].

[24] The generally negative Walén slopes in Figure 5 were obtained during times of tailward $\Delta V_m > 0$ changes between the boundary layer jets and the magnetosheath velocity and mostly east-west directed magnetic fields on either side of the magnetopause. This indicates that C1 was located tailward of an X-line in a region where a positive normal magnetic field is expected since the upstream magnetosheath plasma is assumed to flow into the magnetosphere at the X-line. The antiparallel directions between the flow and the magnetic field result in a negative Walén slope [*Sonnerup et al.*, 1981]. As suggested by the estimated normal magnetic field in the bottom panel of Figure 4, it appears that $B_n$ is generally positive during these times.

[25] A spacecraft located sunward of an X-line would observe a positive Walén slope during these east-west dominated magnetic fields since the normal magnetic field is expected to be earthward ($B_n < 0$) if we assume that the magnetosheath plasma flows earthward across the magnetopause. Moreover, the predicted $\mathbf{j} \times \mathbf{B}$ force would be directed sunward in this region, suggesting that the decelerated tailward flows ($\Delta V_m < 0$) observed near 0512 UT and at subsequent times may be caused by an X-line located tailward of C1. A mostly negative $B_n$ is seemingly also observed during most of these decelerated flow events (see Figure 4).

[26] Note also that all of the estimated HT velocities in Figure 5 are directed tailward, including the decelerated flow event. This indicates that all the proposed X-lines are propagating tailward [e.g., *Gosling et al.*, 1991] over the much slower spacecraft and that the open flux tubes were generated at a reconnection site sunward of C1.

[27] We also performed the Walén analysis over the time period 0440 UT to 0720 UT by sliding a time window of 60 s duration in 4-s incremental steps. The resulting regression slopes, correlation coefficients, $D/D_0$ ratios, and the HT velocities are displayed in Figure 6. As expected from Figure 5, we find that most of the selected plasma jet intervals (between the vertical lines in Figure 6) occur when the conditions of low $D/D_0$ ratios (note the logarithmic scale) and regression slopes near ±1.0 coincide with high correlation coefficients. It seems that the quality of the HT frames are relatively worse for the decelerated flow events than for the accelerated jets. A closer examination of the convective electric fields is necessary, however, to judge this on an individual basis. We find that the $x$ component of $\mathbf{V}_{HT}$ in Figure 6 is consistently negative which suggests the tailward propagation of any open magnetic flux tube on either side of an X-line during this ∼3-hour period in agreement with the observed super-Alfvénic magnetosheath at Cluster [e.g., *Gosling et al.*, 1991; *Cooling et al.*, 2001].

### 3.2. MHD Simulation

[28] An MHD simulation of this event using the LFM code (see Appendix A) has been performed to examine whether these C1 observations of reconnection could be reconciled with the prediction of antiparallel merging in the MHD sash region as tentatively suggested by equation (1). Figure 7 displays two cross sections of the magnetic field magnitude $|\mathbf{B}|$ taken at the GSM position of C1 just after 0600 UT. The red diamond symbol illustrates the C1 position at this time. The $xy$ plane (Figure 7a) indicates that C1 is in fact making its way outward through a region predicted as the sash which is seen here stretching downtail along the dawnside flank magnetopause as a semicontinuous region of magnetic field minima (color-coded in light blue) that seemingly has its point of origin near the cusp/cleft region. The $yz$ plane (Figure 7b) displays the presence of the SH sash on the duskside as well as indicating a clockwise rotation of the magnetospheric cavity, which is to be expected for these negative IMF $B_y$ conditions (see Figure 2b) [e.g., *Siscoe and Sanchez*, 1987; *Eriksson et al.*, 2002].

[29] A 3-D topological image of the magnetic fields surrounding Cluster and the sash is displayed in Figure 8. Two cross sections of the magnetospheric cavity are also shown, one in the equatorial plane at $z_{GSM} = 0$ and another in the noon-midnight plane at $y_{GSM} = 0$. The outermost boundaries of both planes mark the bow shock. Greenish and yellowish colored regions earthward of the bow shock indicate the magnetosheath plasma regime.

[30] Figure 8 further illustrates a set of selected magnetic flux tubes, with the various colors indicating their different characteristics. Magnetic flux tubes with both ends open and connected to the solar wind are color coded in red. Blue flux tubes on the dawnside are closed, as suggested by their connection to both hemispheres. The yellow field lines, however, are open to the solar wind at one end and connected to the geomagnetic field at the other. These field lines have clearly been opened in the vicinity of the NH dawnside sash as suggested by this MHD simulation and display well-defined kinks that should pull the ones connected to the SH equatorward and tailward. The flux tubes connected to the NH may convect further poleward and duskward before turning due tailward unless the super-Alfvénic magnetosheath flow pulls these flux tubes tailward prior to any such deflection [e.g., *Cowley and Owen*, 1989; *Cooling et al.*, 2001]. We also find that the yellow flux

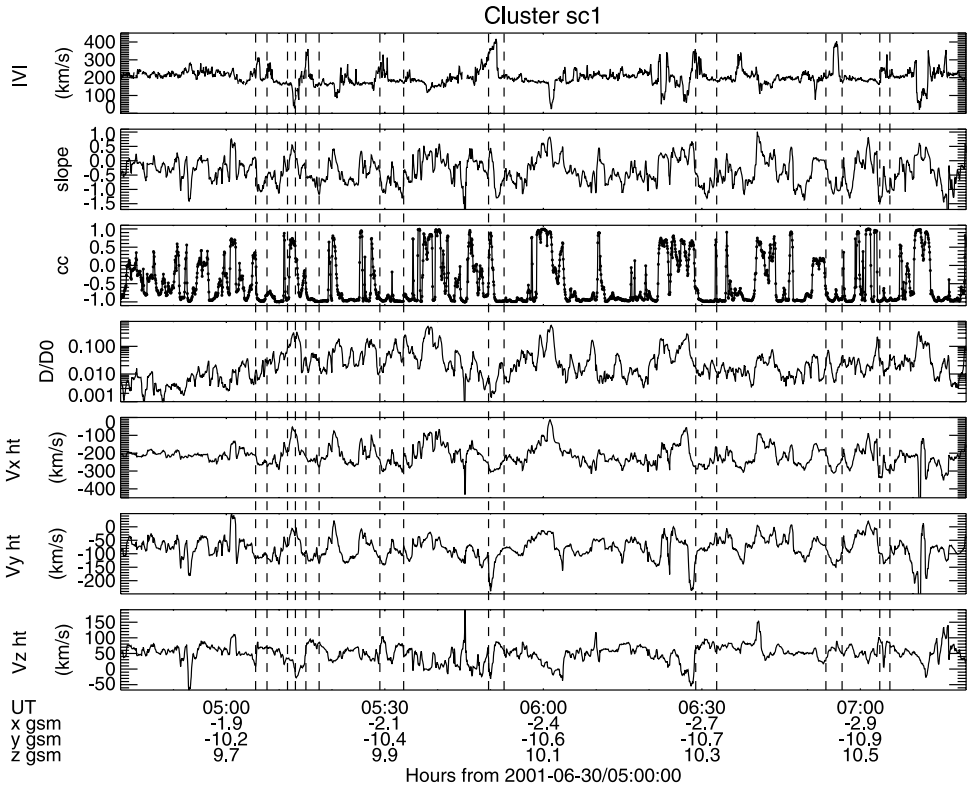


**Figure 6.** Sliding Walén analysis for a time window of 60 s duration from 0440 UT to 0720 UT. The panels from the top depict the magnitude of the ion velocity, regression slope, correlation coefficient, $D/D_0$ quality parameter for the HT frame, and the HT velocity components in GSM coordinates.

tubes intersect the two cross-sectional planes at the approximate magnetopause boundary. The MHD simulations on 30 June thus predict that an antiparallel merging region may exist where a minimum in the magnetic field magnitude occurs on the magnetopause. A detailed comparison between the Cluster observations of $\mathbf{\Delta V}$ and the prediction of antiparallel merging in the MHD sash is performed in section 5 assuming that the velocity change is due to the $\mathbf{j} \times \mathbf{B}$ force from an X-line.

[31] The observed data during a ~94-min interval of the Cluster C1 trajectory starting at 0516:31 UT are compared with the simulated MHD quantities at the corresponding GSM location in Figure 9. The total plasma density, the velocity magnitude, and the magnetic field magnitude are shown in the left column. The MHD simulation reproduces the magnetosheath density very well, except for the density depletions from ~20 $cm^{-3}$ to ~10 $cm^{-3}$ encountered during the partial or complete magnetopause crossings.

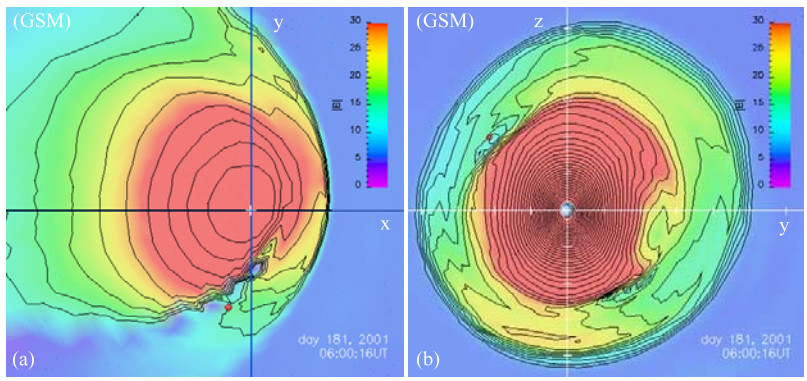


**Figure 7.** MHD simulation results of the magnetic field strength (nT) using the Lyon-Fedder-Mobarry code on 30 June 2001. Data are presented in the GSM coordinate system for two cross sections at ~0600 UT when C1 is located at (−2.4, −10.6, 10.1) $R_E$ (marked by red diamond symbols). (a) The $xy$ plane at $z = 10.1$ $R_E$. (b) The $yz$ plane at $x = -2.4$ $R_E$. Note that C1 is located in a region predicted as the sash as indicated by a weak magnetic field region and color coded in light blue. The magnetotail lobes and the plasma sheet are displayed in red. The outermost boundaries depict the bow shock location.

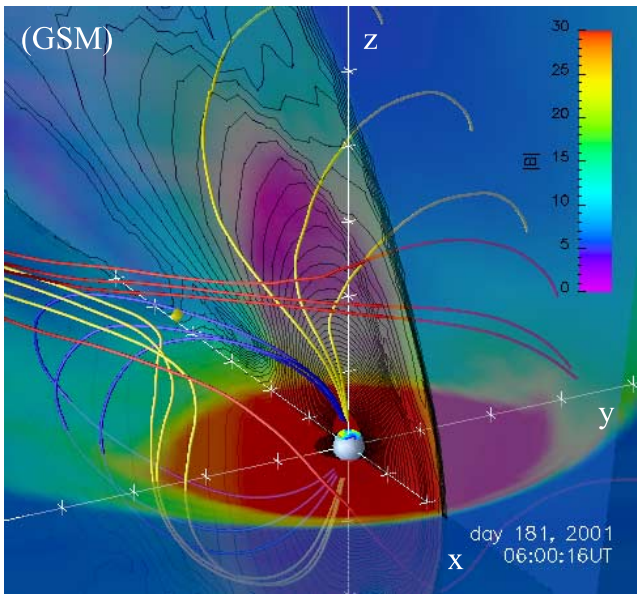


**Figure 8.** A three-dimensional topological view of the MHD magnetosphere and the magnetic fields surrounding C1 (yellow diamond). Same time as in Figure 7. Two cross sections of the magnetosphere are shown at $z = 0$ and $y = 0$, respectively. A selected number of magnetic flux tubes are displayed with red indicating "open-open" fields, blue depicting "closed-closed" fields, and yellow showing "open-closed" flux tubes.

The MHD flow speed is generally overestimated by 30% to 40% in the magnetosheath while none of the observed plasma jets are present in the MHD simulation, at least not along the Cluster trajectory. Moreover, the magnitude of the magnetic field is underestimated by a factor of about 1.5 to 3. Owing to the higher plasma speed and lower magnetic field strength in the MHD flow, it is clear that the simulation results in higher Alfvén Mach numbers than observed by Cluster on the dawnside flank.

[32] The separate GSM components of the velocity and the magnetic field are displayed in the middle and right columns of Figure 9, respectively, and it seems that the $y_{GSM}$ direction of the MHD velocity and magnetic field are better reproduced than the $x_{GSM}$ and $z_{GSM}$ components. The magnetic field rotations detected at the magnetopause crossings are also absent in the MHD simulation.

[33] Most reconnection jets were observed in the proximity of both magnetic field rotations and density depletion regions (see Figure 4). Since these features were absent at these coordinates in the simulation, it may be that the dimension of these structures are smaller than the $\sim$1 $R_E$ spatial resolution of the MHD grid at the dawnside flank. This suggests that the high-speed jets may not be resolved by the MHD simulation, which is also implied by the relatively smoother MHD time series in comparison with the observations. Another possibility is that the virtual Cluster C1 trajectory was located away from the accelerated MHD flows. However, as illustrated in Figure 8, it is clear that the simulated magnetic field displays the topological changes expected in the vicinity of a merging site.

## 4. Southern Hemisphere 29 May Event

[34] The C1 $yz$ position versus $x$ on 29 May 2001 is shown from 0100 UT to 0500 UT in Figure 10 together with the propagated IMF components and the IMF clock angle at the time of this event. The propagation time is $\sim$54 min from the ACE position at (234.7, 40.8, $-11.0$) $R_E$ (GSE) to the subsolar magnetopause at $x = 10$ $R_E$. Unlike the previous event, the IMF $B_y$ is now positive and the Cluster spacecraft are returning toward the dawnside magnetopause in the SH (Figure 10a) at a near-constant clock angle of about $-123°$, while moving from $x = -0.9$ $R_E$ to about $x = -1.8$ $R_E$. The

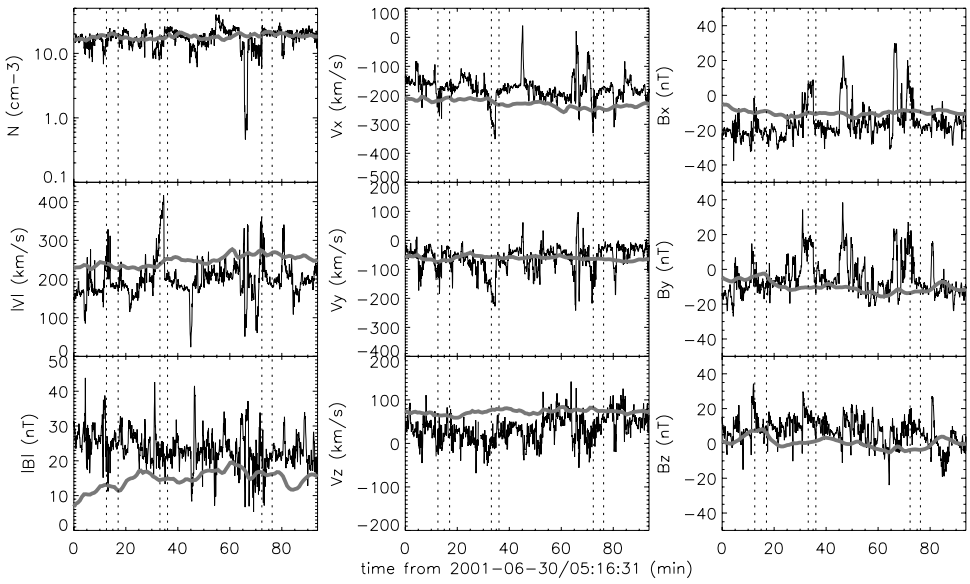


**Figure 9.** Cluster C1 observations (black) of plasma density, velocity, and magnetic field (GSM) are compared with the corresponding MHD parameters (grey) along the virtual trajectory of C1 through the simulation grid between 0516:31 UT and 0650:16 UT.

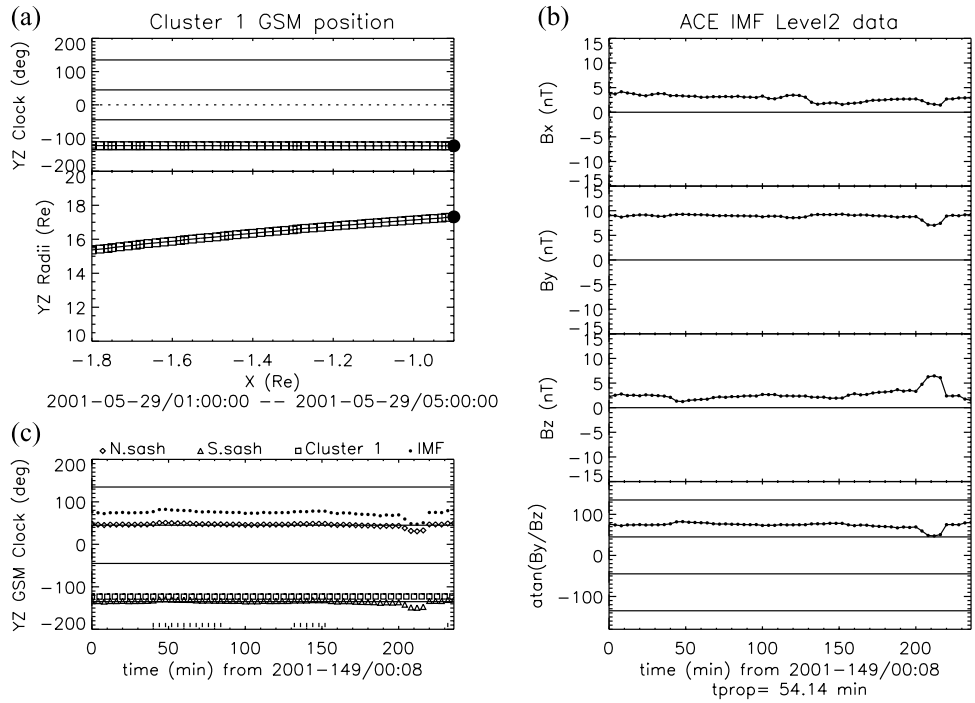


**Figure 10.** C1 position and ACE IMF data on 29 May 2001 from 0100 UT to 0500 UT. Propagation time is ~54 min from ACE to the subsolar point on the magnetopause. Same format as Figure 2. Cluster is predicted to pass within 10° of the SH sash using equation (1) and $\theta_{south} = \theta_{north} + 180°$.

observed IMF clock angle data used as input to equation (1) suggest that C1 moves in the close proximity of the southern sash region on the dawnside flank (Figure 10c).

### 4.1. Cluster Observations

[35] A 2-hour long time interval of C1 data from 0230 UT is shown in Figure 11 (same format as Figure 3). It is seen that C1 moves from the magnetosheath and gradually traverses the magnetopause between 0325 UT and 0330 UT, a time period during which the plasma velocity increases from about 230 km/s and peaks near 360 km/s. It is moreover observed that the magnetosheath Alfvén Mach number (bottom panel) hovers between $M_A = 0.8$ and $M_A = 1.6$ from 0230 UT until 0325 UT. The average Mach number in this time period is $M_A = 1.2$ and the magnetosheath plasma is nearly Alfvénic in contrast to the super-Alfvénic magnetosheath conditions on 30 June (see Figure 3).

[36] The LMN boundary normal directions are estimated by applying the MVA technique to the magnetic field data from C1 between 0321:30 UT and 0341:30 UT (vertical blue lines in Figure 11). The set of eigenvalues resulting from this analysis are $\lambda_1 = 261.67$, $\lambda_2 = 44.88$, and $\lambda_3 = 2.69$, with an intermediate to minimum eigenvalue ratio of 16.70. The corresponding GSM based eigenvectors across this boundary are then rotated about the magnetopause normal direction to an LMN coordinate system with unit vectors $\hat{\mathbf{n}}$ = (0.37, −0.67, −0.64), $\hat{\mathbf{l}}$ = (0.31, −0.56, 0.76), and $\hat{\mathbf{m}}$ = (−0.87, −0.49, 0.00). We then transform the observed **V** and **B** from GSM to the boundary normal LMN frame of reference using these unit vectors. The result is displayed in Figure 12, where three time intervals are shown individually bounded by dashed vertical lines. We observe that the $V_l$ components are increased in the positive $\hat{\mathbf{l}}$ direction (equatorward relative to C1) above the background magnetosheath velocity flow in all three intervals. The three jets also coincide with a depletion in the magnetosheath density as the $B_l$ component rotates northward. The simultaneous $V_m$ components are either enhanced in the positive $\hat{\mathbf{m}}$ direction (third interval) or even accelerated in the negative $\hat{\mathbf{m}}$ direction (first interval). These plasma jets thus indicate a source mainly poleward (southward) of the Cluster spacecraft.

[37] The results from the Walén analysis applied to the three time periods in Figure 12 are shown separately in Figure 13. The HT velocity in GSM coordinates and the $D/D_0$ ratios together with the best fit slopes and the correlation coefficients are once again given in the figure. The Walén slopes in these time intervals range between 0.90 and 1.01 with a correlation coefficient of 0.97. It is therefore concluded, together with the low $D/D_0$ ratios, that these regions of plasma jetting are in very good agreement with that expected for a rotational discontinuity at the magnetopause.

[38] The positive slopes together with the observed directions of the magnetic field (Figures 11–12) further indicate that these observations were detected north of a reconnection X-line where the predicted normal magnetic field across the magnetopause is directed earthward ($B_n < 0$). A negative $B_n$ or an earthward turning normal is also indicated in the bottom panel of Figure 12 during these jets. This is in good agreement with the deduction of the source being below the spacecraft toward the Southern Pole. Note also that the open flux tubes consistently propagate in the

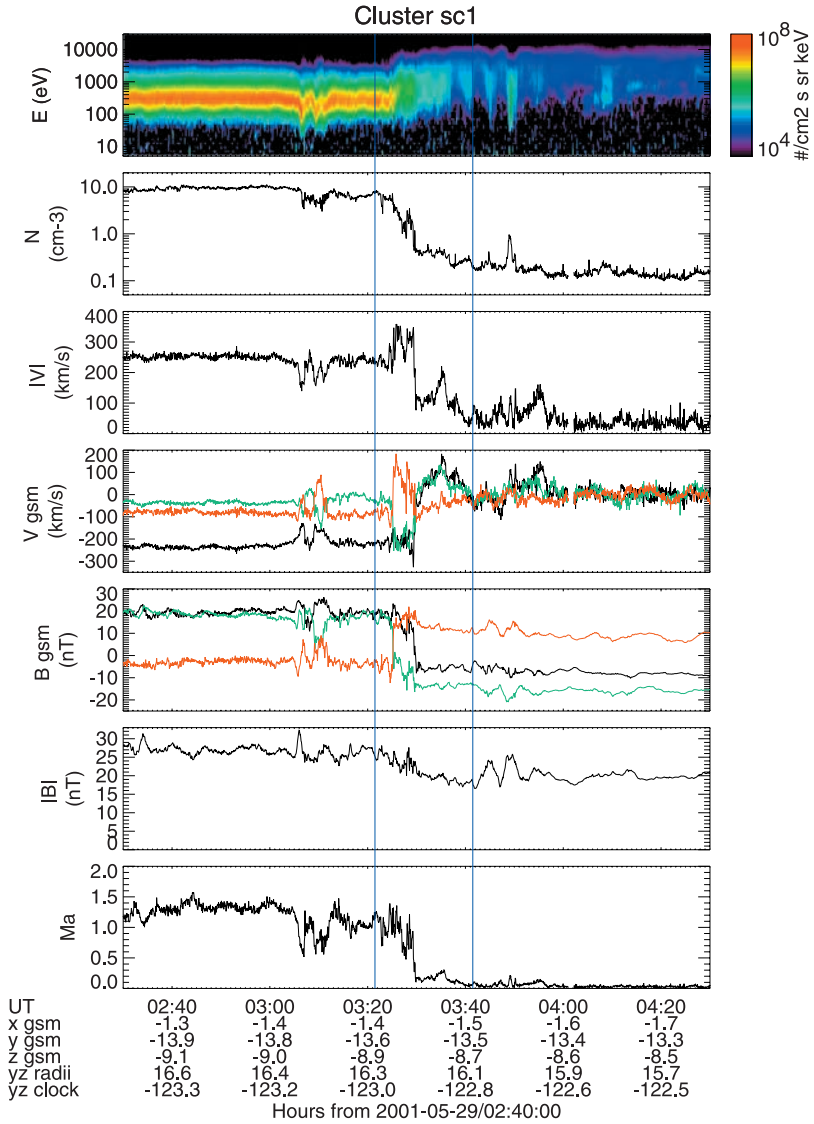


**Figure 11.** Spin resolution C1 data between 0230 UT and 0430 UT from the CIS and FGM instruments on 29 May 2001. Same format as Figure 3. The spacecraft approaches the dawnside magnetosphere from the magnetosheath and gradually traverses the SH magnetopause between 0325 UT and 0330 UT. Blue vertical lines mark the time period of the minimum variance analysis.

tailward and southward direction as suggested by the estimated HT velocities.

### 4.2. MHD Simulation

[39] When simulating this positive IMF $B_y$ event in the framework of the LFM MHD code, we find that the MHD sash is present on the SH dawnside magnetopause and on the NH duskside magnetopause. Figure 14 shows the relative position between C1 (black diamonds) and the southern sash in two GSM cross sections of the simulated magnetosphere. The *xy* plane (Figure 14a) and the *yz* plane (Figure 14b) have been cut at the corresponding *z* and *x* locations of C1 at ~0311 UT. As suggested by the Cluster observations at this time (Figures 11–12), we would expect C1 to be in the magnetosheath on its way earthward toward the magnetopause. This is clearly reproduced by the MHD simulation. Furthermore, it is observed that most of the southern sash region is found below the spacecraft, as is the estimated source region of the observed reconnection jets. A comparison between the directions of $\Delta\mathbf{V}$ in GSM and the location of the MHD sash is given in section 5.

## 5. Discussion

[40] The Cluster observations on 30 June 2001 strongly indicate that a majority of the tailward accelerated flow events are caused by magnetic reconnection. However, there are also a number of time intervals when decelerated flows are observed (see Figure 4). These flows generally seem to fail the Walén test in the HT frame of reference, although the Walén slope is consistently positive (e.g., Figure 5). The decelerated flow signatures often seem to occur prior to the tailward jets and during the initial period of a depleted boundary layer which is detected earthward of the magnetopause based on the direction of the magnetic field as C1 effectively moves from the higher-density magnetosheath.

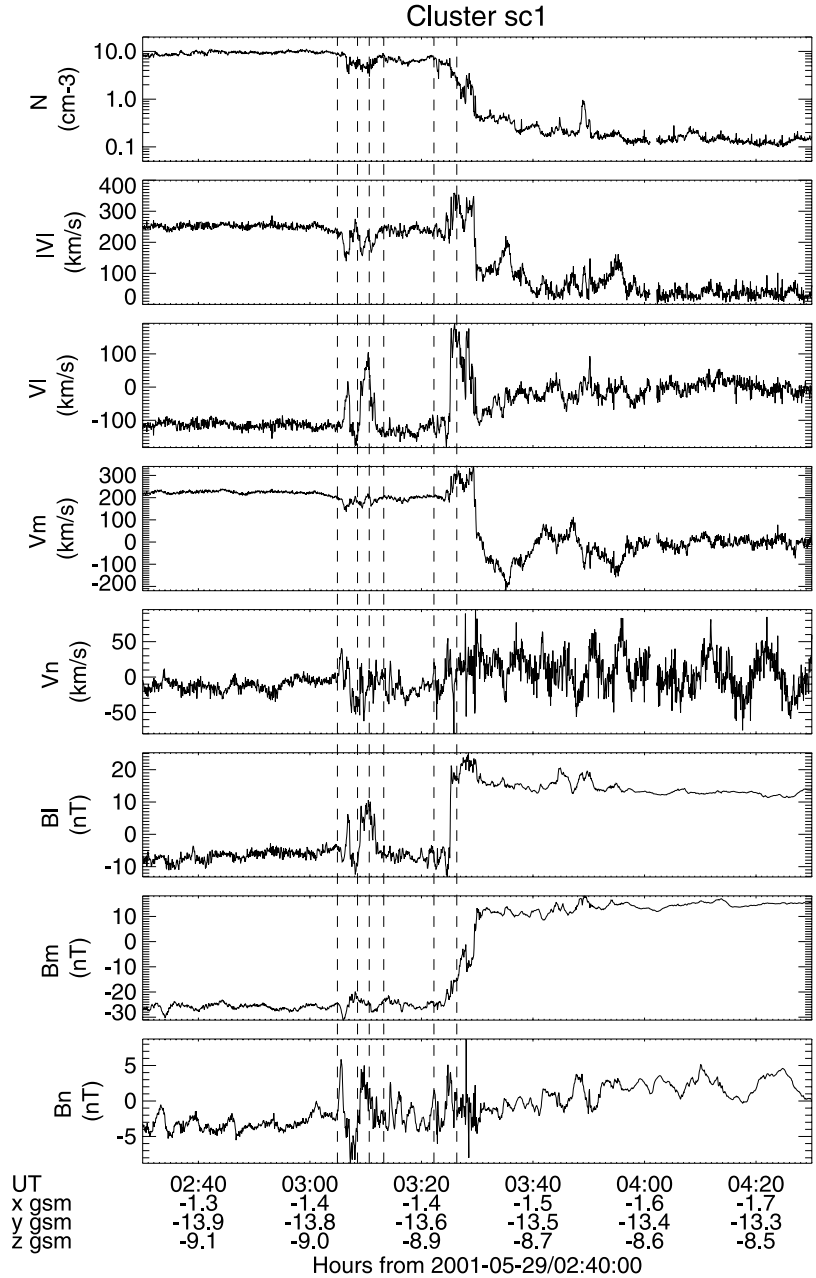


**Figure 12.** C1 ion velocity and magnetic field data detected on 29 May 2001 are shown between 0230 UT and 0430 UT in GSM and transformed into the separate LMN components. Same format as Figure 4. Three regions of enhanced plasma velocity are shown between the dashed vertical lines.

[41] Whether the decelerated flows are the signature of the magnetospheric plasma regime or not is examined in Figure 15, which displays the 4-s resolution plasma and magnetic field data between 0440 UT and 1000 UT (see Figure 3). We identify accelerated flows (green) whenever $|\mathbf{V}| \geq 285$ km/s and the ion plasma $\beta > 0.6$. A subset of decelerated flows (red) is likewise defined when $\beta > 0.6$ and $|\mathbf{V}| \leq 150$ km/s. Figures 15a–15d confirm that both subsets have comparable plasma density (Figure 15a), plasma $\beta$ (Figure 15b), plasma pressure $P_p$ (Figure 15c), and magnetic field pressure $P_b$ (Figure 15d). Moreover, the decelerated flows are clearly separate from the low-density and high-magnetic field pressure region of the magnetosphere at similar velocity magnitudes (e.g., Figures 15a and 15d).

[42] Subsets of the magnetosheath and the magnetosphere may also be identified in Figures 15e–15f using the local LMN coordinate system, which is estimated near 0550 UT (see section 3.1 and Figure 3). The bulk of the magnetospheric distribution is found near $V_m \sim 100$ km/s and for $B_m < 0$ while an average magnetosheath distribution is observed near $V_m \sim 200$ km/s and mostly during $B_m > 0$. It is assumed that the applied LMN system may serve as an approximate boundary normal frame of reference for the magnetopause during the entire interval. This is likely a better approximation for the accelerated (green) and decel-

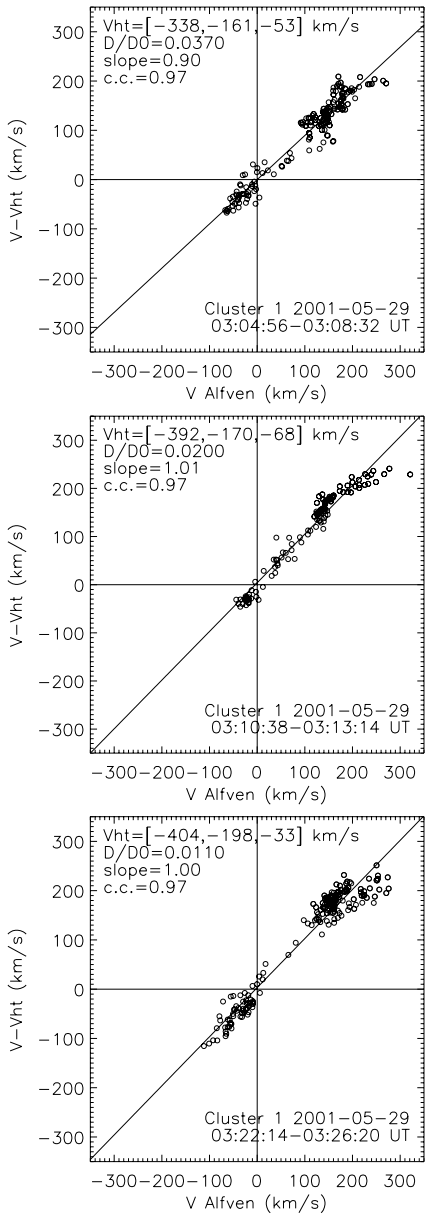


**Figure 13.** Walén analyses for three time periods on 29 May 2001 as indicated in Figure 12. The flow velocity vector in the HT frame is shown versus the Alfvén velocity vector. The correlation coefficient, the best fit slope, the quality ratio of the HT frame $D/D_0$, and the HT velocity are all shown explicitly for each time period. The positive slopes indicate that these observations were detected on the northward side of a reconnection X-line.

erated (red) flows that generally occur between 0500 UT and 0750 UT (see Figures 3–4).

[43] Figure 15f suggests that $B_m < 0$ and $B_n \geq 0$ during most of the accelerated flows which is in good agreement with the negative Walén slopes in Figure 5 and the tailward acceleration of the ions [*Sonnerup et al.*, 1981]. Table 1 presents the statistical distribution of $B_m$ and $B_n$ for the accelerated and decelerated flow distributions as defined above. The results are also compared with $B_m$ and $B_n$ for the estimated bulk of the magnetospheric and the magnetosheath distributions. The magnetospheric subset is defined as $|\mathbf{V}| < 175$ km/s and $\beta \leq 0.6$ and the magnetosheath subset is estimated as $150 < |\mathbf{V}| < 285$ km/s and $\beta > 0.6$. The four subsets thus defined incorporate ~98% of all 4769 data points in the 0440 UT to 1000 UT time period. Table 1 suggests that $B_n \geq 0$ during 70% of the accelerated flows, whereas $B_n < 0$ during 72% of the decelerated flows. This is clearly different from the average properties of either the magnetosheath or the magnetospheric subsets which are mainly separated according to the direction of $B_m$. Figure 15 therefore indicates that C1 may have observed the decelerated flows generated on the sunward side of a reconnection X-line due to the sunward directed $\mathbf{j} \times \mathbf{B}$ force as previously suggested by the positive Walén slopes (e.g., Figure 5) in the HT frame of reference.

[44] Whether a rotational discontinuity is present or not across the magnetopause may also be tested qualitatively in the inertial frame of reference according to the relation $\Delta\mathbf{V} = \pm\Delta\mathbf{B}/\sqrt{\rho_s\mu_0}$ [e.g., *Sonnerup et al.*, 1981, 1990; *Phan et al.*, 2004]. Here, $\Delta\mathbf{V} = \mathbf{V}_{BL} - \mathbf{V}_s$, where $\mathbf{V}_{BL}$ is the average ion velocity measured in the immediate vicinity of the peak velocity (maximum or minimum) that likely occurs within the depleted boundary layer. The reference velocity $\mathbf{V}_s$ is the average magnetosheath velocity evaluated during a ~50-s to ~100-s long interval prior to or after the plasma jet depending on accessibility to a well-defined magnetosheath. The change $\Delta\mathbf{B} = \mathbf{B}_{BL} - \mathbf{B}_s$ is the corresponding difference in the magnetic field and an average magnetosheath mass density $\rho_s$ is used to convert $\Delta\mathbf{B}$ to a change in the Alfvén velocity. As during the HT frame analyses, it is assumed that the magnetosheath consists of 100% $H^+$ and that the plasma pressure is approximately isotropic. Table 2 displays $\mathbf{V}_s$, $\mathbf{B}_s$, the plasma density $N_s$, and the Alfvén Mach number $M_A$ in the magnetosheath for a number of accelerated and decelerated flow events on 30 June and 29 May 2001 including the ones illustrated in Figures 5 and 13. The derived differences $\Delta\mathbf{V}$, $\Delta\mathbf{B}$, and $\Delta\mathbf{V}_A$ (all GSM) relative to the magnetosheath for these events are shown in Table 3.

[45] Figure 16 presents the GSM components of $\Delta\mathbf{V}$ versus $\Delta\mathbf{V}_A$ from Table 3. The tailward acceleration ($\Delta V_x < 0$) on 30 June shown in Figure 16a and the northward ($\Delta V_z > 0$) acceleration on 29 May in Figure 16c compare well with the predicted negative and positive Walén slopes (dashed diagonal lines) previously obtained in the HT frame (see Figure 5 and Figure 13). The positive slope that generally results for the five periods of decelerated ($\Delta V_x > 0$) flows on 30 June (see Figure 16b) therefore suggest the presence of an X-line tailward of Cluster in good qualitative agreement with the indicated earthward $B_n < 0$ direction of the normal magnetic field. It is noted that the components of the average $\Delta\mathbf{V}$ and $\Delta\mathbf{B}$ should be in phase in this region. This is not the case, however, since the $y$, $x$, and $z$ components for the 0521 UT, 0538 UT, and 0651 UT events are out of phase, respectively. In all cases, we would expect an opposite phase for the $\Delta\mathbf{B}$ components.

[46] A possible reason for the difference in magnitude between the positive Walén slopes obtained in the HT frame (Figure 5) and those in the inertial frame (Figure 16b) may be the assumption of 100% $H^+$ when performing this test. This seemed to be an acceptable approach for the tailward accelerated flows independently of the chosen frames of reference. A relatively higher fraction of $O^+$ present on the

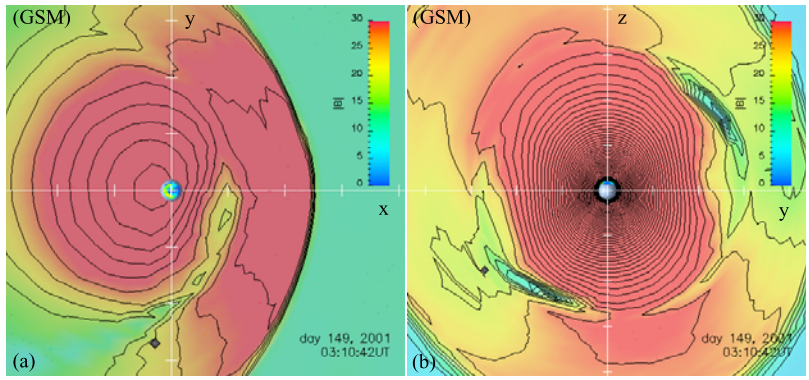


**Figure 14.** MHD simulation results of the magnetic field strength (nT) using the Lyon-Fedder-Mobarry code on 29 May 2001. Data are presented in the GSM coordinate system for two cross sections at ~0311 UT when C1 is located at (−1.4, −13.7, −9.0) $R_E$ (marked by black diamond symbols). (a) The *xy* plane at $z = -9.0$ $R_E$. (b) The *yz* plane at $x = -1.4$ $R_E$. C1 is located in the magnetosheath and just equatorward of a region predicted as the sash. The magnetotail lobes and the plasma sheet are displayed in red as is sections of the magnetosheath. The outermost boundaries depict the bow shock location.

sunward side of the X-line is a possible explanation for the asymmetry if we assume a more direct coupling to the ionospheric $O^+$ source. The presence of $O^+$ would effectively decrease the local Alfvén velocity and result in a steeper Walén slope. Another reason for the asymmetry may be a relatively higher degree of turbulence in the magnetic field on the sunward side of the X-line caused either by the earthward obstacle of the stronger geomagnetic field [e.g., *Priest and Forbes*, 2000] or generated by the opposing directions of the magnetosheath flow and the $\mathbf{j} \times \mathbf{B}$ force that could result in the presence of more complex two-dimensional or three-dimensional magnetic field structures than otherwise assumed in the HT frame analysis [*Sonnerup et al.*, 1990].

[47] We now examine the approximate directions to the reconnection X-line in the inertial frame of reference based on the velocity observations on 30 June and 29 May. It is assumed that the acceleration $\Delta\mathbf{V}$ is primarily due to the $\mathbf{j} \times \mathbf{B}$ force. The given GSM directions of $\Delta\mathbf{V}$ in Table 3 are used to derive a direction $\mathbf{R}_X = -\Delta\mathbf{V}/|\Delta\mathbf{V}|$ to the suggested X-lines. Figure 17 displays the resulting normalized directions of the 12 jets on 30 June (Figures 17a–17c) and the three 29 May jets (Figures 17d–17f) in the $xy_{GSM}$, $yz_{GSM}$, and $xz_{GSM}$ planes, respectively.

[48] When comparing the relative position of Cluster and the location of the MHD sash in the $xy_{GSM}$ plane on 30 June (see Figure 7a) with the estimated X-line directions (Figure 17a), we find a near-perfect agreement with the

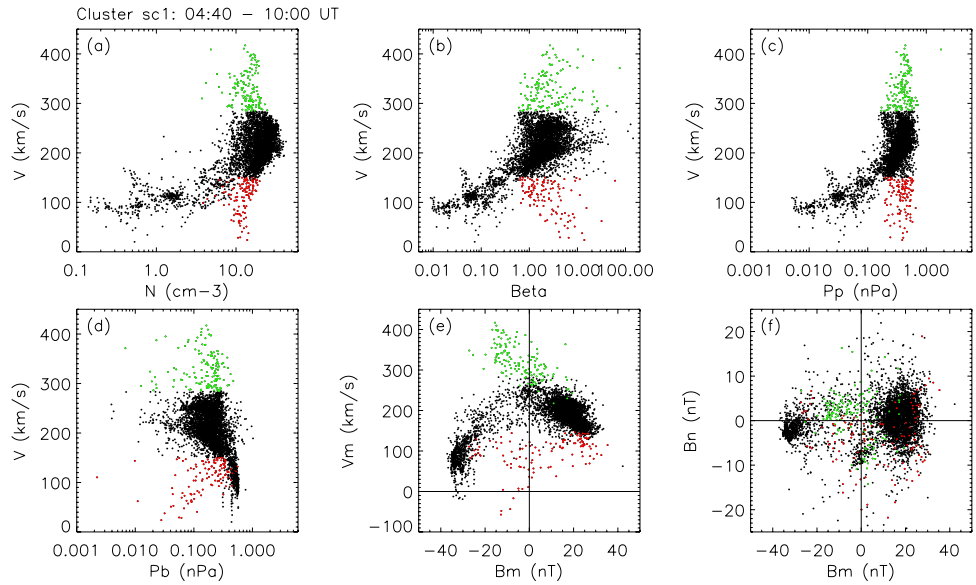


**Figure 15.** Cluster C1 4-s resolution HIA and FGM data are shown for the time interval 0440 UT to 1000 UT on 30 June 2001 (see Figure 3). (a) Velocity magnitude versus plasma density, (b) ion β, (c) plasma pressure $P_p$, (d) magnetic field pressure $P_b$, respectively. The LMN boundary normal system is used to show (e) the $V_m$ versus $B_m$ distribution and (f) the $B_n$ versus $B_m$ distribution. Green and red subsets indicate the tailward and sunward accelerated flows (see text for details).

**Table 1.** Statistical Distribution of $B_n$ and $B_m$ Data Points For the Time Period 0440 UT to 1000 UT on 30 June 2001 in Figure 15f[a]

| | $\Delta V_x < 0$[b] | $\Delta V_x > 0$[c] | Magnetosphere | Magnetosheath |
|---|---|---|---|---|
| $B_n \geq 0$ & $B_m < 0$ | 80 | 13 | 56 | 149 |
| $B_n \geq 0$ & $B_m \geq 0$ | 22 | 21 | 18 | 1950 |
| $B_n < 0$ & $B_m \geq 0$ | 31 | 55 | 18 | 1450 |
| $B_n < 0$ & $B_m < 0$ | 13 | 31 | 508 | 236 |

[a]See text for subset definitions.
[b]$\Delta V_x < 0$ corresponds to tailward accelerated events.
[c]$\Delta V_x > 0$ corresponds to decelerated events.

assumption of antiparallel merging in the MHD sash. However, since C1 is predicted to pass through the central region of the sash in the $yz_{GSM}$ plane, we do not expect any preferred direction to the X-lines in this plane. This is evident from Figures 17b–17c, where $\mathbf{R}_X$ is generally aligned in the $x$ and the $y$ directions and offset only somewhat in the northward direction. A corresponding comparison between $\mathbf{R}_X$ and the sash location on 29 May (see Figure 14) suggests a very similar result, although the best agreement is now seen in the $yz_{GSM}$ plane (Figure 14b and Figure 17e) with the suggested X-lines located below C1 in agreement with the positive Walén slopes in Figure 13 and the position of the sash.

[49] A noticeable difference between the NH and the SH events is that C1 observes reconnection jets from X-lines located either sunward or tailward of it during the 30 June event but detects only jets from X-lines located tailward of C1 on 29 May. Considering that the HT velocity is directed generally in the tailward direction for both events (see Figures 5 and 13), it is likely that the X-lines passed over the Cluster spacecraft on 30 June, whereas open flux tubes connected to only one hemisphere were observed on 29 May. This difference may be attributed to the fact that C1 is located farther away from the source region on 29 May than on 30 June as suggested by the MHD simulations on these dates. It may also be that the relatively larger magnetosheath Mach numbers observed on 30 June (see Table 2) effectively forced the open flux tubes connected to both hemispheres (see Figure 8) due tailward. The generally lower $M_A$ on 29 May may have allowed for a diverging north-south motion of the open flux tubes on either side of the X-lines.

[50] The motion of newly merged flux tubes over the magnetopause is assumed to be determined by magnetic tension due to reconnection and the tugging of the magnetosheath flow acting on the flux tubes [e.g., *Gosling et al.*, 1991; *Cooling et al.*, 2001; *Petrinec and Fuselier*, 2003]. If the magnetosheath flow $V_s$ adjacent to the predicted reconnection site is super-Alfvénic and $V_s > 2V_A$, we expect tailward accelerated ions and a generally antisunward motion of the newly merged flux tubes on either side of the reconnection site [e.g., *Gosling et al.*, 1991], assuming that reconnection is initiated there at all [*Cooling et al.*, 2001]. Steady-state reconnection for these conditions would lead to a tailward migration of the newly formed X-line. When $V_A < V_s < 2V_A$, it is expected that the ions in the inertial frame are accelerated in the sunward direction sunward of the reconnection site, but with $\Delta V < V_s$ [e.g., *Sonnerup et al.*, 1990]. This would therefore be detected as a deceleration in the observed speed. The merged flux will still move tailward on either side of the X-line, however, as also observed on 30 June by Cluster. Both the accelerated ions and the merged flux sunward of the reconnection site would experience a sunward motion in the inertial frame when $V_s < V_A$ as noted, e.g., by *Gosling et al.* [1991].

**Table 2.** Average Magnetosheath Velocity, Magnetic Field, Plasma Density, and Alfvén Mach Number Near 15 Plasma Jets on 30 June and 29 May 2001

| Time,[a] UT | $V_x$, km/s | $V_y$, km/s | $V_z$, km/s | $B_x$, nT | $B_y$, nT | $B_z$, nT | $N_s$, cm$^{-3}$ | $M_A$ |
|---|---|---|---|---|---|---|---|---|
| *Northern Hemisphere 30 June 2001 Event* | | | | | | | | |
| 0506 | −169.85 | −45.13 | 36.13 | −17.54 | −9.94 | 4.36 | 19.10 | 1.72 |
| 0512 | −152.60 | −49.09 | 31.70 | −21.64 | −10.58 | 3.54 | 17.30 | 1.27 |
| 0516 | −146.81 | −36.17 | 41.13 | −21.01 | −14.83 | 7.82 | 16.44 | 1.10 |
| 0521 | −159.20 | −42.10 | 26.84 | −21.51 | −13.86 | 3.77 | 17.58 | 1.25 |
| 0530 | −185.69 | −54.95 | 7.17 | −19.09 | −11.02 | 7.91 | 18.80 | 1.70 |
| 0538 | −136.06 | −61.22 | 32.19 | −24.17 | −7.87 | 9.02 | 14.39 | 0.98 |
| 0550 | −188.49 | −61.42 | 39.79 | −17.98 | −7.26 | 8.17 | 22.34 | 2.04 |
| 0601 | −166.24 | −36.08 | 33.36 | −21.15 | −5.14 | 7.13 | 17.10 | 1.43 |
| 0630 | −196.13 | −44.09 | 46.68 | −16.56 | −7.76 | 8.59 | 20.76 | 2.13 |
| 0651 | −190.20 | −48.20 | 49.58 | −15.38 | −14.08 | 0.09 | 16.90 | 1.80 |
| 0655 | −174.38 | −49.53 | 40.60 | −15.54 | −13.11 | 2.55 | 23.76 | 2.02 |
| 0705 | −157.69 | −37.51 | 56.74 | −24.65 | −7.36 | 6.28 | 16.84 | 1.22 |
| *Southern Hemisphere 29 May 2001 Event* | | | | | | | | |
| 0307 | −208.75 | −34.16 | −94.29 | 20.40 | 15.09 | −2.83 | 8.82 | 1.23 |
| 0310 | −208.86 | −21.28 | −97.51 | 20.00 | 16.78 | −2.52 | 7.56 | 1.12 |
| 0326 | −210.62 | −26.73 | −65.97 | 18.93 | 17.50 | −1.92 | 5.70 | 0.94 |

[a]These are the approximate times within each of the Walén test intervals.

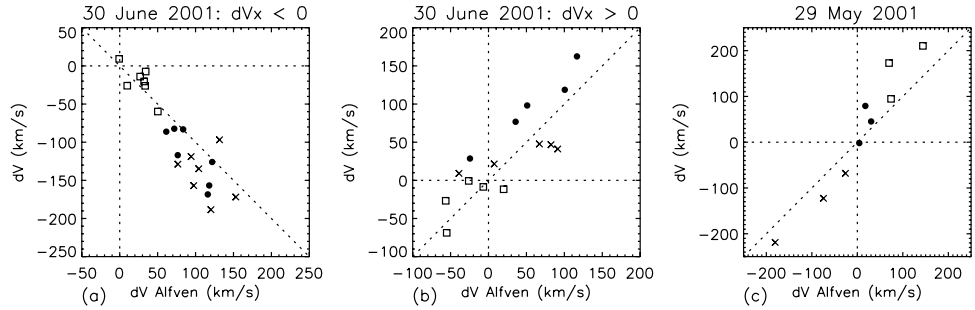


**Figure 16.** The qualitative Walén relation $\Delta\mathbf{V} = \pm\Delta\mathbf{B}/\sqrt{\rho_s\mu_0}$ as performed in the inertial frame of reference for (a) tailward accelerated jets on 30 June 2001, (b) sunward accelerated jets on 30 June, and (c) northward and dawnward accelerated jets on 29 May 2001. Solid dots, crosses, and squares symbolize the *x*, *y*, and *z* GSM components, respectively (see Table 3).

[51] We propose that the near-Alfvénic magnetosheath flows on 29 May allowed for the predominantly equatorward acceleration of the ions, although the merged flux tubes experienced a motion in the tailward direction as seen by the estimated tailward and southward direction of the HT velocities in Figure 13. The observed ion deflection suggests that the reconnection site was located tailward (see Figure 17) but mostly below the Cluster spacecraft, in agreement with the relative location of the simulated MHD sash. It is possible that these jets would have escaped downtail without being detected at C1 for super-Alfvénic magnetosheath flows with $V_s > 2V_A$ since C1 passed away from the core region of the simulated sash (see Figure 14).

[52] The shear angle between the magnetic fields on either side of the magnetopause is estimated when Cluster clearly traverses this boundary as indicated by the plasma density. Here we use the tangential $B_l$ and $B_m$ components of the magnetic field. There are two clear crossings during the 0600 UT to 0720 UT time interval on 30 June (see Figure 4). The first one occurs between 0621:40 UT and 0623:40 UT. The resulting magnetic field shear in the magnetopause LM plane is 177° for the inbound crossing near 0622 UT and 171° for the ~0623:30 UT outbound crossing. The fields are thus within 3° and 9° of being antiparallel. The second magnetopause crossing is a longer lasting event with C1 being earthward of the magnetopause for just over 3 min. Examining the inbound traversal near 0710:30 UT and the outbound traversal at ~0713 UT separately results in shear angles of 171° and 173°, respectively. The magnetic fields are thus within 9° and 7° of being antiparallel. A corresponding analysis for the SH event on 29 May (see Figure 12) results in a shear angle of only 144° across the more gradual magnetopause transition between 0324:05 UT and ~0330 UT.

[53] The data recorded by C1 thus seem to favor antiparallel merging at the Cluster location on 30 June but not during the 29 May event. It should be noted, however, that the actual relative direction of the magnetic fields at the merging site could differ from the shear angles measured at Cluster. It is also observed that Cluster detected jets from either side of the X-lines on 30 June but only from one side of the X-lines on 29 May. This indicates that C1 was much

**Table 3.** Average Changes $\Delta\mathbf{V}$ and $\Delta\mathbf{B}$ Across 15 Plasma Jets on 30 June and 29 May 2001 Relative to the Magnetosheath Parameters in Table 2[a]

| Time,[b] UT | $\Delta V_x$, km/s | $\Delta V_y$, km/s | $\Delta V_z$, km/s | $\Delta B_x$, nT | $\Delta B_y$, nT | $\Delta B_z$, nT | $\Delta V_{Ax}$, km/s | $\Delta V_{Ay}$, km/s | $\Delta V_{Az}$, km/s |
|---|---|---|---|---|---|---|---|---|---|
| *Northern Hemisphere 30 June 2001 Event* | | | | | | | | | |
| 0506 | −83.16 | −118.87 | −20.44 | 16.77 | 18.89 | 6.45 | 83.68 | 94.27 | 32.20 |
| 0512 | 118.68 | 41.10 | −68.73 | 19.18 | 17.41 | −10.52 | 100.56 | 91.29 | −55.15 |
| 0516 | −125.93 | −171.84 | −26.13 | 22.66 | 28.46 | 6.24 | 121.91 | 153.10 | 33.58 |
| 0521 | 76.75 | 9.10 | −0.71 | 6.87 | −7.49 | −5.01 | 35.72 | −38.97 | −26.04 |
| 0530 | −86.22 | −128.79 | 9.25 | 12.21 | 15.26 | −0.14 | 61.41 | 76.75 | −0.69 |
| 0538 | 28.59 | 21.57 | −26.75 | −4.25 | 1.31 | −9.82 | −24.45 | 7.54 | −56.47 |
| 0550 | −156.71 | −156.88 | −25.97 | 25.57 | 21.15 | 2.15 | 118.03 | 97.62 | 9.91 |
| 0601 | 162.44 | 47.64 | −8.57 | 22.11 | 12.73 | −1.30 | 116.63 | 67.14 | −6.86 |
| 0630 | −117.02 | −96.82 | −7.37 | 15.99 | 27.50 | 7.16 | 76.54 | 131.65 | 34.29 |
| 0651 | 98.12 | 46.79 | −11.68 | 9.61 | 15.55 | 3.75 | 50.97 | 82.49 | 19.92 |
| 0655 | −168.43 | −134.81 | −13.98 | 25.96 | 23.30 | 6.03 | 116.14 | 104.26 | 26.99 |
| 0705 | −82.36 | −188.44 | −59.81 | 13.53 | 22.63 | 9.46 | 71.94 | 120.28 | 50.29 |
| *Southern Hemisphere 29 May 2001 Event* | | | | | | | | | |
| 0307 | 79.23 | −67.96 | 94.69 | 2.40 | −3.56 | 10.09 | 17.59 | −26.16 | 74.12 |
| 0310 | 45.29 | −122.57 | 172.89 | 3.82 | −9.39 | 8.80 | 30.31 | −74.48 | 69.80 |
| 0326 | −1.91 | −218.92 | 210.35 | 0.47 | −19.75 | 15.77 | 4.31 | −180.48 | 144.13 |

[a] $\Delta\mathbf{V}_A$ assumes a magnetosheath density $N_s$.
[b] These are the approximate times within each of the Walén test intervals.

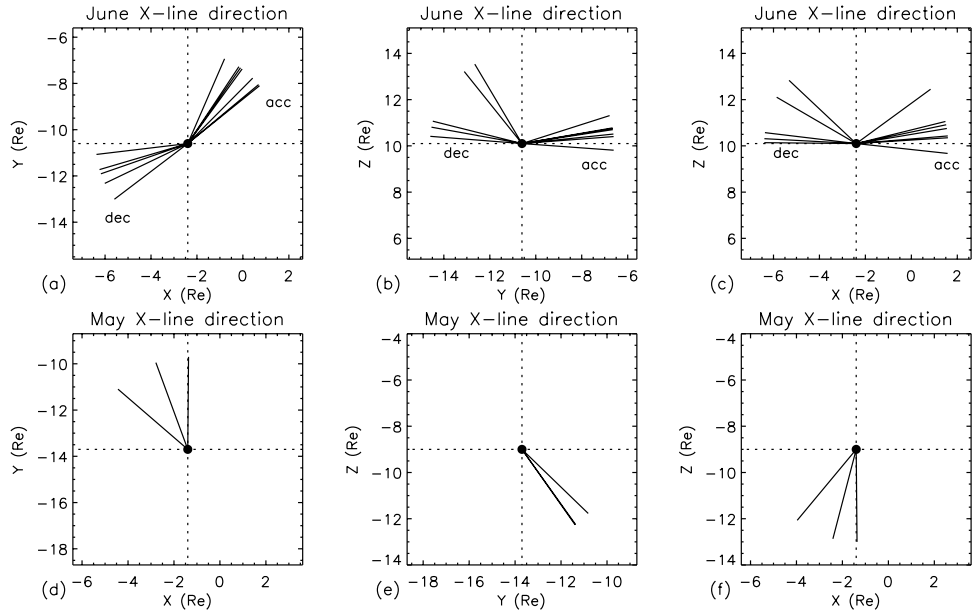


**Figure 17.** The estimated directions to the X-lines $\mathbf{R}_X = -\Delta\mathbf{V}/|\Delta\mathbf{V}|$ in three GSM planes (a–c) on 30 June 2001 and (d–f) on 29 May 2001 based on Table 3. It is assumed that $\Delta\mathbf{V} \sim \mathbf{j} \times \mathbf{B}$. The central solid dots correspond to the C1 positions at (−2.4,−10.6,10.1) $R_E$ on 30 June (∼0600 UT) and at (−1.4, −13.7, −9.0) $R_E$ on 29 May (∼0311 UT).

closer to the neutral line for the NH event than during the SH event as also suggested by the MHD simulations. It is therefore possible that the deviation from antiparallel alignment between the fields on 29 May is due to the spatial separation between C1 and the proposed location of antiparallel merging sites in the MHD sash where these X-lines may have been generated.

[54] As shown by *Cowley and Owen* [1989] and *Cooling et al.* [2001], it is necessary for the magnetosheath flow to be sub-Alfvénic adjacent to a reconnection site tailward of the cusps to achieve steady-state reconnection there during northward IMF. As seen for the NH event that occurred during generally steady northward and predominantly dawnward IMF (see Figures 2–3), reconnection did generate several tailward propagating X-lines distributed over a 2-hour time period. The steady nature of the source region on 30 June is also apparent from a comparison of the estimated HT velocities between ∼0505 UT and ∼0705 UT in Figure 5 with the average $\langle \mathbf{V}_{HT} \rangle = (-274, -108, 76)$ km/s (excluding the decelerated flow event). The average offset is only 2.7° with a mean standard deviation of 1.9°. The HT velocity during the decelerated flow event made an angle of about 13° with $\langle \mathbf{V}_{HT} \rangle$. Moreover, considering that C1 was located in the range $-1.9\ R_E < x_{GSM} < -3.0\ R_E$ during this time period, it is possible that the magnetosheath flow adjacent to the reconnection site sunward of C1 was more Alfvénic or even sub-Alfvénic, allowing for a region of nearly steady-state reconnection [*Cooling et al.*, 2001] that generated the observed tailward propagating X-lines.

[55] The combined results of solar wind driven MHD simulations and observations of reconnection jets on 30 June and 29 May clearly show that accelerated ion flows reach the Cluster spacecraft along a line-of-sight from the simulated MHD sash. Figure 18 further illustrates the expected locations of antiparallel merging and the tilted component merging line at 0610 UT on 30 June 2001 (Figures 18a–18b) and the correspondingly modeled merging regions at 0320 UT on 29 May 2001 (Figures 18c–18d). The antiparallel merging regions (black) illustrate where the magnetic fields are within 10° of being oppositely aligned. The two IMF-based models employ the draping of magnetosheath fields onto the geomagnetic field at the magnetopause as determined by the Tsyganenko T96 model [*Tsyganenko*, 1995] and predict merging sites that generally agree with that of the MHD sash.

[56] We therefore conclude that the Cluster observations together with the MHD simulations and the modeled locations of merging sites strongly support the view that the global distribution of merging on the magnetopause is primarily determined by the direction of the IMF [see also *Phan et al.*, 2000; *Marcucci et al.*, 2000] in contrast to the hypothesis of randomly distributed reconnection sites on the magnetopause as described by, e.g., *Nishida* [1989]. The fact that the plasma flows are consistently observed to be accelerated along the line-of-sight between the sash and C1, which is located 44° north of the equatorial $xy_{GSM}$ plane on 30 June and 33° south of this plane on 29 May, further support this conclusion. If magnetic reconnection occurred randomly over the magnetopause, we would expect at least some of the events to display $\Delta\mathbf{V}$ directions clearly away from the modeled merging regions and the MHD sash.

## 6. Summary and Conclusions

[57] We have performed a detailed study of reconnection signatures on the dawnside flank magnetopause based on Cluster observations in the Northern Hemisphere on 30 June 2001 and in the Southern Hemisphere on 29 May 2001. The evidence consists of field-aligned flows at the Alfvén speed in the deHoffmann-Teller frame of reference during times of

accelerated or decelerated plasma flows (relative to the magnetosheath) as expected for rotational discontinuities. The plasma jets tend to occur during periods of depleted magnetosheath densities in agreement with the presence of a reconnection boundary layer [*Sonnerup et al.*, 1981] earthward of the magnetopause.

[58] It is concluded from the near 180° magnetic shear angles and the tailward propagation of the X-lines over the Cluster C1 spacecraft in the Northern Hemisphere that the plasma jets were generated at an antiparallel merging site on 30 June 2001. The positive Walén slopes and the lower 144° shear angle measured at Cluster C1 on 29 May 2001 may suggest a component merging site south of Cluster.

[59] However, the measured directions of the plasma jets $\Delta\mathbf{V}$ in either hemisphere are well correlated with the relative locations of C1 and the predicted regions of antiparallel merging based on MHD simulations for these events. Cluster C1 was also found further away from these MHD regions on 29 May than on 30 June. It is therefore possible that the magnetic fields were more antiparallel at the merging site that generated these jets than what was observed at Cluster.

[60] A direct comparison between Cluster measurements and a simulation of MHD parameters such as density, velocity, and magnetic fields along an approximate 90 min long section of the C1 trajectory failed to reproduce the observed plasma jets and the corresponding magnetic field rotations and plasma density depletions. This may be related to the relatively low $\sim 1 R_E$ spatial resolution of the MHD grid on the flanks. It may also be that the predicted location of the MHD magnetopause is different from what is observed. However, based on the connection between magnetic flux tubes from the magnetosheath with those of magnetospheric origin on the Northern Hemisphere dawnside flank, it is clear that the simulated magnetic field topology is consistent with magnetic reconnection in these dawnside regions where antiparallel merging is predicted. These observations demonstrate that global merging on the dayside magnetopause is primarily governed by the direction of the magnetosheath magnetic field as implied by Cluster measurements and the IMF.

## Appendix A: Lyon-Fedder-Mobarry MHD Code

[61] The Lyon-Fedder-Mobarry (LFM) code is a global model used for simulating the interaction of a solar wind driver on the coupled magnetosphere-ionosphere system. It uses the ideal magnetohydrodynamic equations to describe the behavior of the plasma within the solar wind and magnetosphere. The ionosphere is treated as a two-dimensional electrostatic system which is coupled to the magnetosphere via a set of empirical relationships. This description provides a self-consistent physical model of the system.

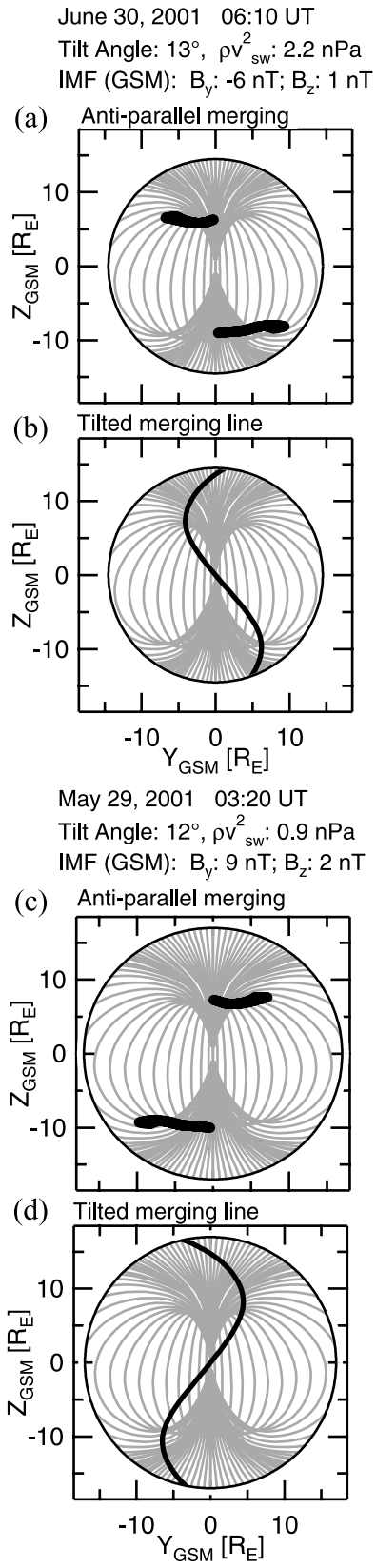


**Figure 18.** Semiempirically modeled regions of (a) antiparallel merging and (b) the tilted component merging line as projected onto the magnetopause (view from the Sun) are displayed for the solar wind conditions on 30 June 2001 at 0610 UT. The corresponding (c) antiparallel and (d) component merging regions at 0320 UT on 29 May 2001 are also shown. The magnetosheath field is draped over the geomagnetic field which is determined using the Tsyganenko 1996 model [*Tsyganenko*, 1995].

[62] The simulation solves the ideal MHD equations in conservative form,

$$\frac{\partial \rho}{\partial t} + \nabla \cdot (\rho \vec{v}) = 0 \tag{A1}$$

$$\frac{\partial \rho \vec{v}}{\partial t} + \nabla \cdot \left[ \rho \vec{v}\, \vec{v} + \left( p + \frac{B^2}{8\pi} \right) \bar{I} - \frac{\vec{B}\vec{B}}{4\pi} \right] = 0 \tag{A2}$$

$$\frac{\partial \vec{B}}{\partial t} + \nabla \cdot \left( \vec{v}\vec{B} - \vec{B}\vec{v} \right) = 0 \tag{A3}$$

$$\frac{\partial \rho E}{\partial t} + \nabla \cdot \left[ \vec{v} \left( \rho E + p + \frac{B^2}{8\pi} \right) - \vec{B} \left( \vec{v} \cdot \vec{B} \right) \right] = 0, \tag{A4}$$

with the total energy, $E$, in equation (A4) defined as

$$E \equiv \frac{1}{2} \rho v^2 + \frac{p}{\gamma + 1} + \frac{B^2}{8\pi}. \tag{A5}$$

[63] This formulation is used since it is well adapted to finite volume numerical methods for hyperbolic systems, which have been shown to be much more robust and accurate than any of the alternatives which have been applied to MHD. Moreover, Adams-Bashforth time marching is applied with a centered eighth-order spatial differencing. In addition, nonlinear numerical switches based on the partial donor method [*Hain*, 1987] are used to maintain a total variance diminishing (TVD) solution. Methods to fulfill this TVD condition were developed for systems of equations (J. G. Lyon et al., unpublished memo, 1983) while still maintaining the numerical divergence of the magnetic field equal to zero. These techniques are used on a distorted cylindrical mesh [*Wiltberger et al.*, 2000] which has an axis that extends from a front boundary at $x = 30\ R_E$ to the rear boundary at $x = -350\ R_E$ where the radius is $100\ R_E$. This mesh has been designed to place resolution in regions known a priori to be important, e.g., the magnetopause, bow shock, and magnetotail. The smallest sizes that are resolved in these regions are approximately $0.33\ R_E$.

[64] The magnetospheric simulation has an inner boundary at $3\ R_E$ and is coupled to an ionospheric simulation which solves

$$J_{\parallel} = \nabla_{\perp} \cdot \left( \bar{\Sigma} \cdot \vec{E_I} \right) \tag{A6}$$

as an equation for the ionospheric potential. The conductivity matrix, $\bar{\Sigma}$, includes the solar EUV ionization as well as local enhancements that are determined from empirical relationships between the MHD parameters at the inner edge of the computational grid and the Hall and Pedersen conductivities [*Wiltberger et al.*, 2003, and references therein]. Once the electric field in the ionosphere is determined, it is mapped back along dipole field lines to the inner boundary of the MHD regime and is used as boundary condition on the plasma flow.

[65] **Acknowledgments.** The first author SE would like to thank the PIs on the CIS and FGM teams and Melvyn L. Goldstein at NASA Goddard Space Flight Center for making this data set available for analysis. We thank the ACE team for the solar wind data via http://www.srl.caltech.edu/ACE/ASC/level2/ and Elsa Chrétien at CESR in Toulouse, France, for providing ascii files of the CIS ion energy-time spectrograms. This research was conducted under NASA grants NAG5-12026 and NNG04GH82G.

[66] Lou-Chuang Lee thanks Antonius Otto and Joachim Raeder for their assistance in evaluating this paper.

## References

Avanov, L. A., V. N. Smirnov, J. H. Waite Jr., S. A. Fuselier, and O. L. Vaisberg (2001), High-latitude magnetic reconnection in sub-Alfvénic flow: Interball Tail observations on May 29, 1996, *J. Geophys. Res.*, *106*, 29,491–29,502.

Balogh, A., et al. (2001), The Cluster magnetic field investigation: Overview of in-flight performance and initial results, *Ann. Geophys.*, *19*, 1207–1217.

Cooling, B. M. A., C. J. Owen, and S. J. Schwartz (2001), Role of the magnetosheath flow in determining the motion of open flux tubes, *J. Geophys. Res.*, *106*, 18,763–18,775.

Cowley, S. W. H., and C. J. Owen (1989), A simple illustrative model of open flux tube motion over the dayside magnetopause, *Planet. Space Sci.*, *37*, 1461–1475.

Crooker, N. U. (1979), Dayside merging and cusp geometry, *J. Geophys. Res.*, *84*, 951–959.

Crooker, N. U., G. L. Siscoe, and F. R. Toffoletto (1990), A tangent subsolar merging line, *J. Geophys. Res.*, *95*, 3787–3793.

deHoffmann, F., and E. Teller (1950), Magnetohydrodynamic shocks, *Phys. Rev.*, *80*, 692.

Dungey, J. W. (1961), Interplanetary magnetic field and the auroral zones, *Phys. Rev. Lett.*, *6*, 47.

Eriksson, S., J. W. Bonnell, L. G. Blomberg, R. E. Ergun, G. T. Marklund, and C. W. Carlson (2002), Lobe cell convection and field-aligned currents poleward of the region 1 current system, *J. Geophys. Res.*, *107*(A8), 1185, doi:10.1029/2001JA005041.

Escoubet, C. P., M. Fehringer, and M. Goldstein (2001), The Cluster mission, *Ann. Geophys.*, *19*, 1197–1200.

Gonzalez, W. D., and F. S. Mozer (1974), A quantitative model for the potential resulting from reconnection with an arbitrary interplanetary magnetic field, *J. Geophys. Res.*, *79*, 4186–4194.

Gosling, J. T., M. F. Thomsen, S. J. Bame, R. C. Elphic, and C. T. Russell (1991), Observations of reconnection of interplanetary and lobe magnetic field lines at the high-latitude magnetopause, *J. Geophys. Res.*, *96*, 14,097–14,106.

Hain, K. (1987), The partial donor method, *J. Comput. Phys.*, *73*, 131.

Kessel, R. L., S.-H. Chen, J. L. Green, S. F. Fung, S. A. Boardsen, L. C. Tan, T. E. Eastman, J. D. Craven, and L. A. Frank (1996), Evidence of high-latitude reconnection during northward IMF: Hawkeye observations, *Geophys. Res. Lett.*, *23*, 583–586.

Khrabrov, A. V., and B. U. Ö. Sonnerup (1998), DeHoffmann-Teller analysis, in *Analysis Methods for Multi-Spacecraft Data*, edited by G. Paschmann and P. W. Daly, *ISSI Sci. Rep., SR-001*, p. 221–248, ESA Publ. Div., Noordwijk, Netherlands.

Lockwood, M., B. S. Lanchester, H. U. Frey, K. Throp, S. K. Morley, S. E. Milan, and M. Lester (2003), IMF control of cusp proton emission intensity and dayside convection: Implications for component and anti-parallel reconnection, *Ann. Geophys.*, *21*, 955–982.

Luhmann, J. G., R. J. Walker, C. T. Russell, N. U. Crooker, J. R. Spreiter, and S. S. Stahara (1984), Patterns of potential magnetic field merging sites on the dayside magnetopause, *J. Geophys. Res.*, *89*, 1739–1742.

Marcucci, M. F., et al. (2000), Evidence for interplanetary magnetic field $B_y$ controlled large-scale reconnection at the dayside magnetopause, *J. Geophys. Res.*, *105*, 27,497–27,507.

Maynard, N. C., et al. (2001), Observation of the magnetospheric "sash" and its implications relative to the solar-wind/magnetospheric coupling: A multisatellite event analysis, *J. Geophys. Res.*, *106*, 6097–6122.

Nishida, A. (1989), Can random reconnection on the magnetopause produce the low-latitude boundary layer?, *Geophys. Res. Lett.*, *16*, 227–230.

Nishikawa, K.-I. (1998), Particle entry through reconnection grooves in the magnetopause with a dawnward IMF as simulated by a 3-D EM particle code, *Geophys. Res. Lett.*, *25*, 1609–1612.

Paschmann, G., B. U. Ö. Sonnerup, I. Papamastorakis, N. Sckopke, G. Haerendel, S. J. Bame, J. R. Asbridge, J. T. Gosling, C. T. Russell, and R. C. Elphic (1979), Plasma acceleration at the Earth's magnetopause: Evidence for magnetic reconnection, *Nature*, *282*, 243.

Petrinec, S. M., and S. A. Fuselier (2003), On continuous versus discontinuous neutral lines at the dayside magnetopause for southward interplanetary magnetic field, *Geophys. Res. Lett.*, *30*(10), 1519, doi:10.1029/2002GL016565.

Phan, T. D., et al. (2000), Extended magnetic reconnection at the Earth's magnetopause from detection of bi-directional jets, *Nature*, *404*, 848–850.

Phan, T. D., B. U. Ö. Sonnerup, and R. P. Lin (2001), Fluid and kinetics signatures of reconnection at the dawn tail magnetopause: Wind observations, *J. Geophys. Res.*, *106*, 25,489–25,501.

Phan, T. D., et al. (2004), Cluster observations of continuous reconnection at the magnetopause under steady interplanetary magnetic field conditions, *Ann. Geophys.*, *22*, 1–13.

Priest, E., and T. Forbes (2000), *Magnetic Reconnection: MHD Theory and Applications*, Cambridge Univ. Press, New York.

Rème, H., et al. (2001), First multispacecraft ion measurements in and near the Earth's magnetosphere with the identical Cluster ion spectrometry (CIS) experiment, *Ann. Geophys.*, *19*, 1303–1354.

Russell, C. T., and R. C. Elphic (1979), ISEE observations of flux transfer events at the dayside magnetopause, *Geophys. Res. Lett.*, *6*, 33–36.

Shue, J.-H., et al. (1998), Magnetopause location under extreme solar wind conditions, *J. Geophys. Res.*, *103*, 17,691–17,700.

Siscoe, G. L., and E. Sanchez (1987), An MHD model for the complete open magnetotail boundary, *J. Geophys. Res.*, *92*, 7405–7412.

Siscoe, G. L., G. M. Erickson, B. U. Ö. Sonnerup, N. C. Maynard, K. D. Siebert, D. R. Weimer, and W. W. White (2001), Magnetospheric sash dependence on IMF direction, *Geophys. Res. Lett.*, *28*, 1921–1924.

Sonnerup, B. U. Ö. (1971), Magnetopause structure during the magnetic storm of September 24, 1961, *J. Geophys. Res.*, *76*, 6717.

Sonnerup, B. U. Ö. (1974), Magnetopause reconnection rate, *J. Geophys. Res.*, *79*, 1546–1549.

Sonnerup, B. U. Ö., and M. Scheible (1998), Minimum and maximum variance analysis, in *Analysis Methods for Multi-Spacecraft Data*, edited by G. Paschmann and P. W. Daly, *ISSI Sci. Rep., SR-001*, p. 185–220, ESA Publ. Div., Noordwijk, Netherlands.

Sonnerup, B. U. Ö., G. Paschmann, I. Papamastorakis, N. Sckopke, G. Haerendel, S. J. Bame, J. R. Asbridge, J. T. Gosling, and C. T. Russell (1981), Evidence for magnetic field reconnection at the Earth's magnetopause, *J. Geophys. Res.*, *86*, 10,049–10,067.

Sonnerup, B. U. Ö., I. Papamastorakis, G. Paschmann, and H. Lühr (1987), Magnetopause properties from AMPTE/IRM observations of the convection electric field: Method development, *J. Geophys. Res.*, *92*, 12,137–12,159.

Sonnerup, B. U. Ö., I. Papamastorakis, G. Paschmann, and H. Lühr (1990), The magnetopause for large magnetic shear: Analysis of convection electric fields from AMPTE/IRM, *J. Geophys. Res.*, *95*, 10,541–10,557.

Tsyganenko, N. A. (1995), Modeling the Earth's magnetospheric magnetic field contained within a realistic magnetopause, *J. Geophys. Res.*, *100*, 5599–5612.

White, W. W., G. L. Siscoe, G. M. Erickson, Z. Kaymaz, N. C. Maynard, K. D. Siebert, B. U. Ö. Sonnerup, and D. R. Weimer (1998), The magnetospheric sash and the cross-tail S, *Geophys. Res. Lett.*, *25*, 1605–1608.

Wiltberger, M., T. I. Pulkkinen, J. G. Lyon, and C. C. Goodrich (2000), MHD simulation of the magnetotail during the December 10, 1996, substorm, *J. Geophys. Res.*, *105*, 27,649–27,663.

Wiltberger, M., J. G. Lyon, and C. C. Goodrich (2003), Results from the Lyon-Fedder-Mobarry global magnetospheric model for the electrojet challenge, *J. Atmos. Sol. Terr. Phys.*, *65*, 1213–1222.

Yeh, T. (1976), Dayside reconnection between a dipolar geomagnetic field and a uniform interplanetary field, *J. Geophys. Res.*, *81*, 2140–2144.

M. André, Swedish Institute of Space Physics, Box 537, SE-75121, Uppsala, Sweden.

A. Balogh, The Blackett Laboratory, Imperial College, Prince Consort Road, London, SW7 2BZ, UK.

M. W. Dunlop, Space Sciences Division, Rutherford Appleton Laboratory, Chilton, Didcot, Oxfordshire, OX11 0QX, UK.

S. R. Elkington, R. E. Ergun, and S. Eriksson, Laboratory for Atmospheric and Space Physics, University of Colorado, 1234 Innovation Drive, Boulder, CO 80303, USA. (scot.elkington@lasp.colorado.edu; eriksson@lasp.colorado.edu)

S. M. Petrinec, Lockheed Martin Advanced Technology Center, 3251 Hanover Street, Palo Alto, CA 94304-1191, USA. (petrinec@spasci.com)

T. D. Phan, Space Sciences Laboratory, University of California, Berkeley, Centennial Drive at Grizzly Peak Blvd, Berkeley, CA 94720-7450, USA. (phan@ssl.berkeley.edu)

H. Rème, Centre d'Etude Spatiale des Rayonnements, 9 Ave du Colonel Roche, 31028, Toulouse cedex 4, France.

M. Wiltberger, High Altitude Observatory, National Center for Atmospheric Research, 3450 Mitchel Lane, Boulder, CO 80301, USA.